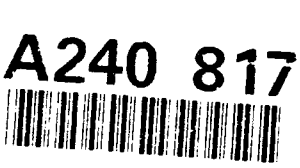

JR+E Report 91073

MICROSTRUCTURAL STUDY OF CLOTH-REINFORCED CARBON-CARBON LAMINATES

J. Jortner, S. W. Yurgartis, and K. Morey

Final Report

to

Office of Naval Research
Attn: Dr. S. G. Fishman, Code 1131
800 N. Quincy Street
Arlington, VA 22217

under

Contract N00014-82-C-0405

Submitted by

Jortner Research & Engineering, Inc
P. O. Box 2825
Costa Mesa, CA 92628-2825

June 1991

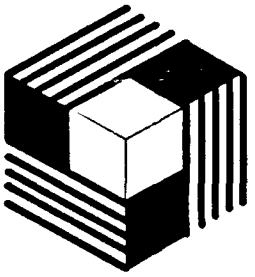

JR+E

Unclassified
SECURITY CLASSIFICATION OF THIS PAGE

REPORT DOCUMENTATION PAGE

Form Approved OMB No. 0704-0188

1a. REPORT SECURITY CLASSIFICATION: Unclassified	1b. RESTRICTIVE MARKINGS: None
2a. SECURITY CLASSIFICATION AUTHORITY: N/A	3. DISTRIBUTION/AVAILABILITY OF REPORT: Approved for Public Release; Distribution Unlimited
2b. DECLASSIFICATION/DOWNGRADING SCHEDULE: N/A	
4. PERFORMING ORGANIZATION REPORT NUMBER(S): JR+E 91073	5. MONITORING ORGANIZATION REPORT NUMBER(S):
6a. NAME OF PERFORMING ORGANIZATION: Jortner Research & Engineering; 6b. OFFICE SYMBOL (If applicable):	7a. NAME OF MONITORING ORGANIZATION: Office of Naval Research
6c. ADDRESS (City, State, and ZIP Code): P O Box 2825, Costa Mesa, CA 92628	7b. ADDRESS (City, State, and ZIP Code): 800 N. Quincy St, Arlington, VA 22217-5000
8a. NAME OF FUNDING/SPONSORING ORGANIZATION: Office of Naval Research; 8b. OFFICE SYMBOL (If applicable): ONR	9. PROCUREMENT INSTRUMENT IDENTIFICATION NUMBER: N00014-82-C-0405
8c. ADDRESS (City, State, and ZIP Code): 800 N. Quincy St, Arlington, VA 22217-5000	10. SOURCE OF FUNDING NUMBERS: PROGRAM ELEMENT NO. NR; PROJECT NO. 039; TASK NO. 235; WORK UNIT ACCESSION NO.

11. TITLE (Include Security Classification)

MICROSTRUCTURAL STUDY OF CLOTH-REINFORCED CARBON-CARBON LAMINATES

12. PERSONAL AUTHOR(S): J. Jortner, S. W. Yurgartis, and K. Morey

13a. TYPE OF REPORT	13b. TIME COVERED	14. DATE OF REPORT (Year, Month, Day)	15. PAGE COUNT
Final	FROM 2/89 TO 12/90	910630	vi + 82

16. SUPPLEMENTARY NOTATION

17. COSATI CODES			18. SUBJECT TERMS (Continue on reverse if necessary and identify by block number)
FIELD	GROUP	SUB-GROUP	composite materials; carbon-carbon composites; microstructure; processing; image analysis; cloth reinforcement

19. ABSTRACT (Continue on reverse if necessary and identify by block number)

The microstructure of cloth-reinforced carbon-carbon laminates was studied, with emphasis on features observable at relatively low magnifications, such as: the geometric shape of fiber bundles (yarns), yarn crimp, fiber orientations, nesting of cloth layers, and minimechanical microcracking. The development of these features during processing is discussed, with the aid of observations made with a hot-stage-equipped microscope. Computer-aided digital image analysis techniques are applied to the quantification of yarn shapes. Further quantifications of microstructures are recommended as relevant to improved understanding of the links among processing, microstructure, and thermomechanical behavior of carbon-carbon materials.

20. DISTRIBUTION/AVAILABILITY OF ABSTRACT: ☒ UNCLASSIFIED/UNLIMITED ☐ SAME AS RPT. ☐ DTIC USERS	21. ABSTRACT SECURITY CLASSIFICATION: Unclassified
22a. NAME OF RESPONSIBLE INDIVIDUAL: Dr. S. G. Fishman	22b. TELEPHONE (Include Area Code): 703-696-0285; 22c. OFFICE SYMBOL: ONR Code 1131

DD Form 1473, JUN 86 Previous editions are obsolete. SECURITY CLASSIFICATION OF THIS PAGE: Unclassified

FOREWORD

The work discussed here was conducted at Jortner Research & Engineering, Inc., Costa Mesa, California, and at Clarkson University, Potsdam, New York. The principal investigator was Julius Jortner. The work at Clarkson University was directed by Prof. Steven W. Yurgartis and performed with the aid of his student Mr. Kevin Morey.

Dr. L. H. Peebles, Jr., served as the scientific officer at the Office of Naval Research, from this contract's inception until his retirement in 1990. Dr. Steven G. Fishman then served as ONR's scientific officer.

The report contains three chapters. Numbering of figures and references is started anew with each chapter.

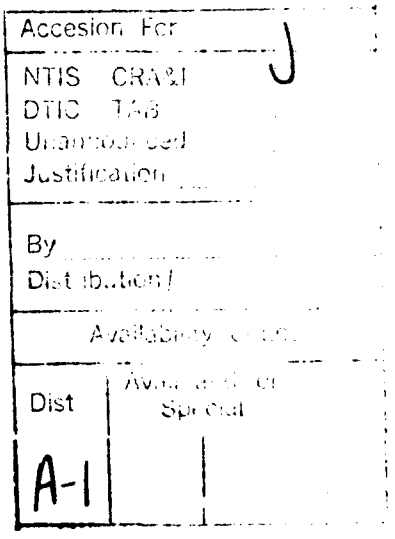

TABLE OF CONTENTS

CHAPTER 1

MICROSTRUCTURE OF CLOTH-REINFORCED CARBON-CARBON LAMINATES

The paper that follows has been accepted for publication by the journal Carbon. It provides a summary of observations that predate the application of the image-analysis techniques described in Chapter 3.

MICROSTRUCTURE OF CLOTH-REINFORCED CARBON-CARBON LAMINATES*

Julius Jortner
Jortner Research & Engineering, Inc.
Costa Mesa, California 92628-2825

Abstract

Fiber-bundle orientations and microcracking in cloth-reinforced carbon-carbon laminates are described, with emphasis on the development of these features during composite fabrication. Microscope examinations of plain-weave cloth, and of laminates made from the cloth, show the interwoven yarns undergo complex distortions of shape during fabrication of laminates; various nesting possibilities are noted. Differences, attributed to details of the weave, are observed between the responses of fill-yarn and warp-yarn crimp angles to laminate compaction. Development of microcracks, which traverse fiber bundles in carbon-carbons, is studied during the first carbonization heating of a phenolic-resin matrix in plain-weave and satin-weave laminates. The statistical nature of microstructural descriptors, like crimp angles and microcrack spacings, is emphasized. Further quantitative studies of fiber orientation and microcracking are recommended as relevant to improved understanding of the processing and the thermomechanical behavior of cloth-reinforced carbon-carbons.

Key Words

Carbon-carbon composites, crimp, microcracks, cloth, woven reinforcements

---

* Based on a lecture at the 6th Annual Conference on Materials Technology, Southern Illinois University at Carbondale, April 1990.

1. INTRODUCTION

Many carbon-carbon laminates of interest for structural applications are reinforced with woven cloth. Significant microstructural features include:

a. Fiber orientations.

The yarns comprising the reinforcing cloth are wavy because they pass over and under each other. The yarns themselves are frequently made of two or more plies twisted about each other. Therefore, the filaments locally are at various orientations to the nominal material axes (the warp, fill and crossply directions). Fiber orientations may be affected also by yarn movements during compaction of cloth layers during lamination. Details of fiber-bundle orientation are known to affect strength and stress-strain response [1-4].

b. Microcracks.

Microcracking, an inevitable result of matrix shrinkage during carbonization and the thermal-expansion anisotropy of unidirectional carbon-carbon [5], may be viewed on two levels: at high magnification on the scale of a filament diameter (micromechanical viewpoint); and at low magnification on the scale of the cloth layer thickness or yarn diameter (minimechanical viewpoint). The micromechanical view focuses on cracking in matrix and at fiber-matrix interfaces within a fiber bundle; such observations [6,7] may be related to load transfer among fibers and the transverse properties of fiber bundles. The minimechanical view focuses on cracks that traverse significant portions of a fiber bundle, the interface between fiber bundles, an inter-yarn pocket of unreinforced matrix, or the interface between a fiber bundle and a matrix pocket; because the minimechanical cracks affect the load transfer among fiber bundles and among cloth laminae, they are believed to be of major influence on all engineering properties.

This paper describes selected micro-features of two types of laminates: those reinforced with a plain-woven cloth of low-modulus rayon-based carbon yarns, and those reinforced with satin-woven cloth of medium-modulus PAN-based carbon yarns. In both weaves, the warp and fill yarns are nominally perpendicular to each other. The laminates were made (elsewhere) by prepregging the cloth with phenolic resin, stacking layers of cloth so their warp yarns are aligned, compacting and curing the resin-matrix laminate in a pressurized autoclave, carbonizing the laminate by heating to 650°C or more, and densifying further with one or more cycles of impregnation with liquid resin or pitch and carbonization. High-temperature heat treatments (to 2000°C or more), called graphitizations, were applied at one or more intermediate stages and as the final process step.

The focus here is on the effects of processing on fiber-bundle orientations and on minimechanical microcracking. The work is part of an ongoing study aimed at quantifying the microstructural features of carbon-carbons. The longer-range goal is to provide quantitative descriptions of such laminates in a form that would lead to more realistic models of thermostructural behavior.

2. CRIMP ANGLES AND NESTING

Previous work [3] shows that sample-to-sample variations of crimp angles (Fig. 1) in plain-weave laminates correlate to sample tensile strength (Fig. 2). The desire to limit strength variation motivates further study of crimp. The observations described below show crimp angles can be distinctly non-uniform in prepregged cloth, and that the crimp-angle distribution is affected by the compaction of the laminate.

2.1 Plain-Weave Prepreg

Photomicrographs (see [3]) of a plain-weave carbon cloth (known as WCA, made from low-modulus rayon-based yarns by Amoco Performance Products), prepregged with a phenolic resin, were used to construct the sketch of the weave shown in the upper half of Fig. 3. The fill-yarn count is about 22 yarns per

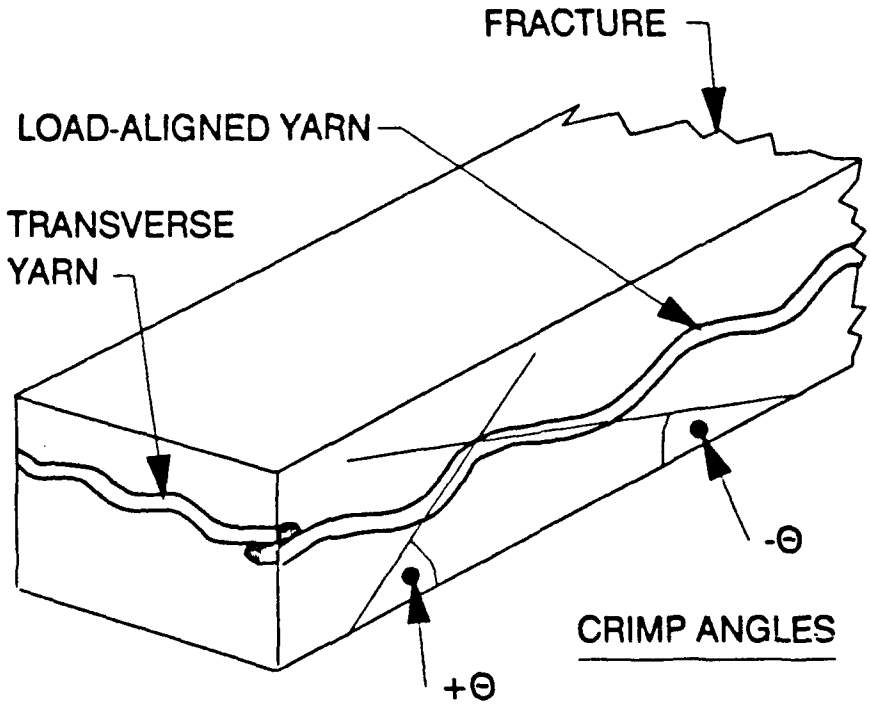

Fig. 1. Definition of crimp angles of a yarn in a plain-weave laminate (after [3]).

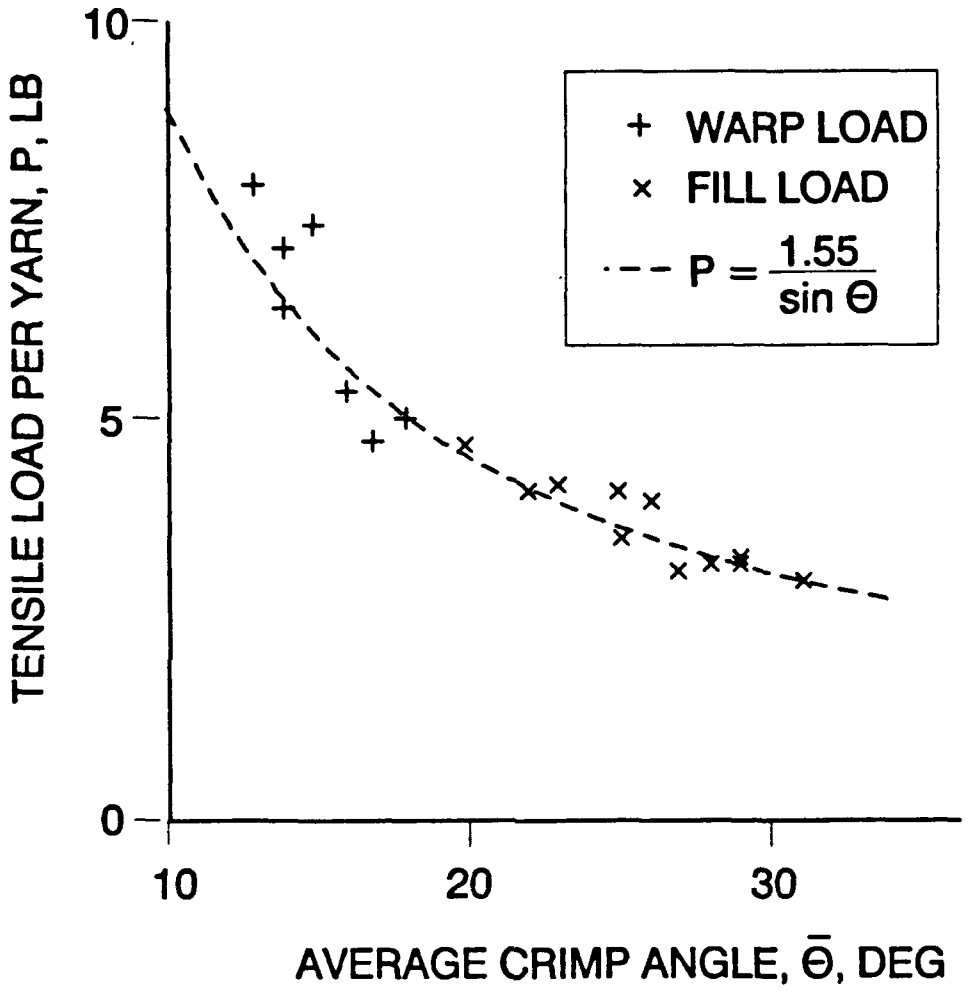

Fig. 2. Correlation of tensile strengths to average crimp angles measured in specimens from several batches of a plain-weave-reinforced carbon-carbon laminate (after [3]). Tensile strength is represented by the load at failure divided by the number of load-oriented yarns in the specimen cross-section. Tests were in the warp (+) and the fill (x) directions.

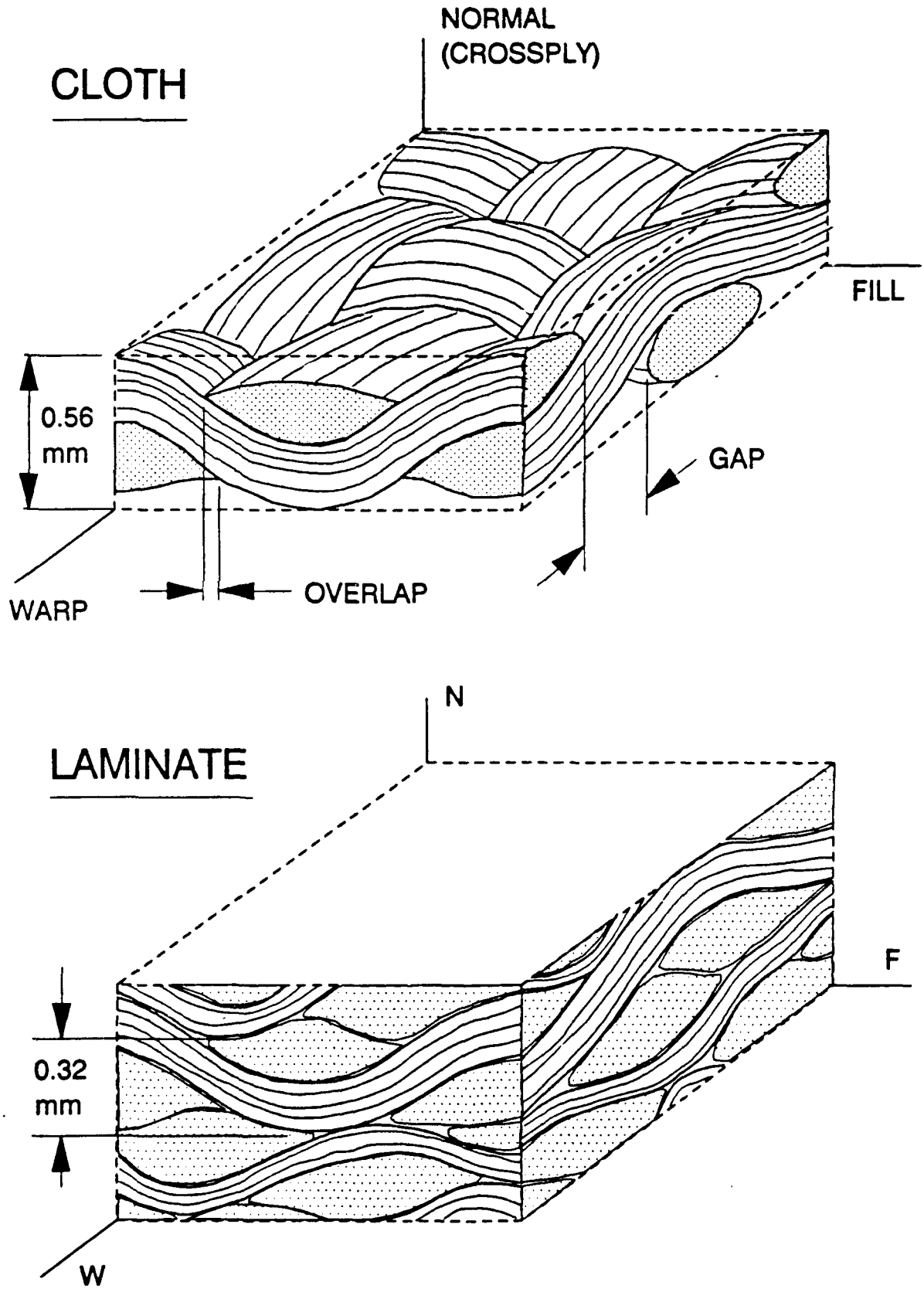

Fig. 3. Plain-weave structure. Upper sketch is of unit cell of WCA cloth. Lower sketch is a representative region of a carbon-carbon laminate made with WCA cloth.

inch (870 per meter) of cloth; the warp count is about 28 yarns per inch (1100 per meter). Fill cross-sections tend to be elliptical, whereas warp cross-sections are asymmetrically lenticular with sharp corners. The crimp angle is about twice as large for the fills as for the warps, presumably a result of greater tension on the warps during some stage of weaving, carbonization, or prepregging. The lesser fill count allows for gaps between neighboring fill yarns, whereas the warps overlap slightly. From Amoco's data [8] for the weight per unit area of WCA cloth and its density measured by helium displacement, and from the volume of the unit cell (the rectangular prism bounded by dashed lines in Fig. 3), the volume fraction of fibers within the unit cell is calculated to be about 31 percent. Assuming fibers occupy about 60 percent of each yarn cross-section, the yarns (as bounded by the outline of their cross-sections) are estimated to occupy less than 55 percent of the unit-cell volume. Thus, there is considerable space for compaction during lamination.

Crimp, defined as the fractional amount by which the yarn length exceeds the cloth length, is estimated as about .02 for the warp yarns and about .08 for the fills; these estimates assume the waveforms in the prepreg are sinusoids. Inasmuch as the fiber lengths cannot change significantly during compaction, changes in yarn geometry during laminate compaction (described in the next section) must be limited to isolength changes in waveform, or must be accommodated by lateral movement of fibers. This issue has not yet been addressed quantitatively; tentatively, we would presume the aforementioned gaps allow easier lateral distortion of fill yarns than of the warps.

2.2 Plain-Weave Laminate

The lower half of Fig. 3 is a sketch of the fully-processed carbon-carbon laminate made with plain-weave prepreg of the type described above. The sketch is based on examination of several photomicrographs. The 0.32-mm dimension indicates approximately the average layer-to-layer spacing. The nesting of layers, caused by compaction of the laminate during cure in a pressurized autoclave, eliminates much of the empty space seen in the unit cell of Fig. 3.

Compaction causes a decrease in the crossply (N-direction) dimensions of the yarns, and is accompanied by lateral shifts of yarn position that are especially noticeable for the fill yarns. The warp yarn cross-sections tend to remain centered in the fill-yarn undulation; the lateral movements of the fill yarns cause distortions of the warp-yarn waveforms so the peaks of the wave are no longer centered between the valleys.

Applying the same fiber data that were used to estimate volume fractions in the prepreg unit cell, to a volume calculated from the yarn wavelengths and the ply spacing in the laminate, it is estimated that the fiber volume fraction within the composite is about 54 percent and that the yarns occupy about 90 percent of the laminate volume. These probably are overestimates because fiber cross-sections may decrease somewhat during heat treatment [9,10].

2.3 Crimp-Angle Statistics

To explore the variability of crimp angles, specimens cut from a sample of plain-weave prepreg (Fig. 4) were cured (without pressure), mounted individually in resin, polished, and examined in a microscope. Each specimen was about 25 mm long. The crimp angles of each undulation on the plane of polish were measured and the averages (of the absolute values) are listed in Fig. 4. In this piece of prepreg, the warp crimp angles vary more than the fill crimp angles.

For the sake of eventually narrowing the variability, it would be worth determining whether most of the observed crimp-angle variation is inherent in the rayon weave, introduced during carbonization of the rayon weave, or introduced during prepregging.

Fig. 5 shows the distribution of crimp angles measured [3] on two specimens from one panel of a fully processed carbon-carbon laminate. Also shown are the distributions of crimp angles in the prepreg sample described above (Fig. 4). Crimp angles in fill yarns of the composite are generally smaller than those in the prepreg, presumably a direct result of compaction; apparently, compaction decreases the amplitude of the fill-yarn waveform without affecting the

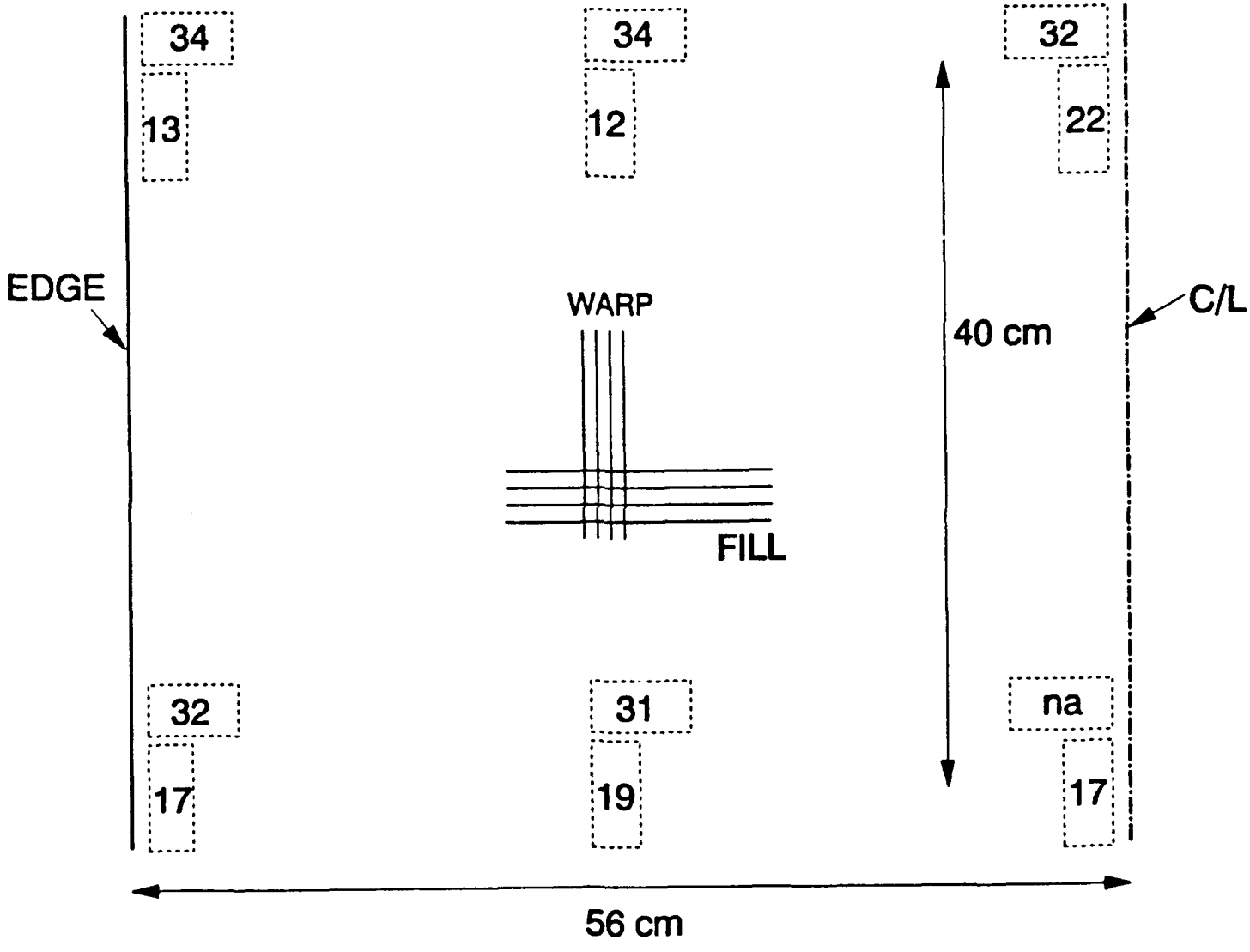

Fig. 4. Sketch of a sample of WCA/phenolic prepreg, about half the width of the carbonized cloth, showing locations of specimens (about 25 mm long by 10 mm wide) for which crimp angles were measured. The numbers represent average crimp angle in each specimen over yarn length of about 25 mm. The average includes positive crimp angles and the absolute value of negative crimp angles (Fig. 1).

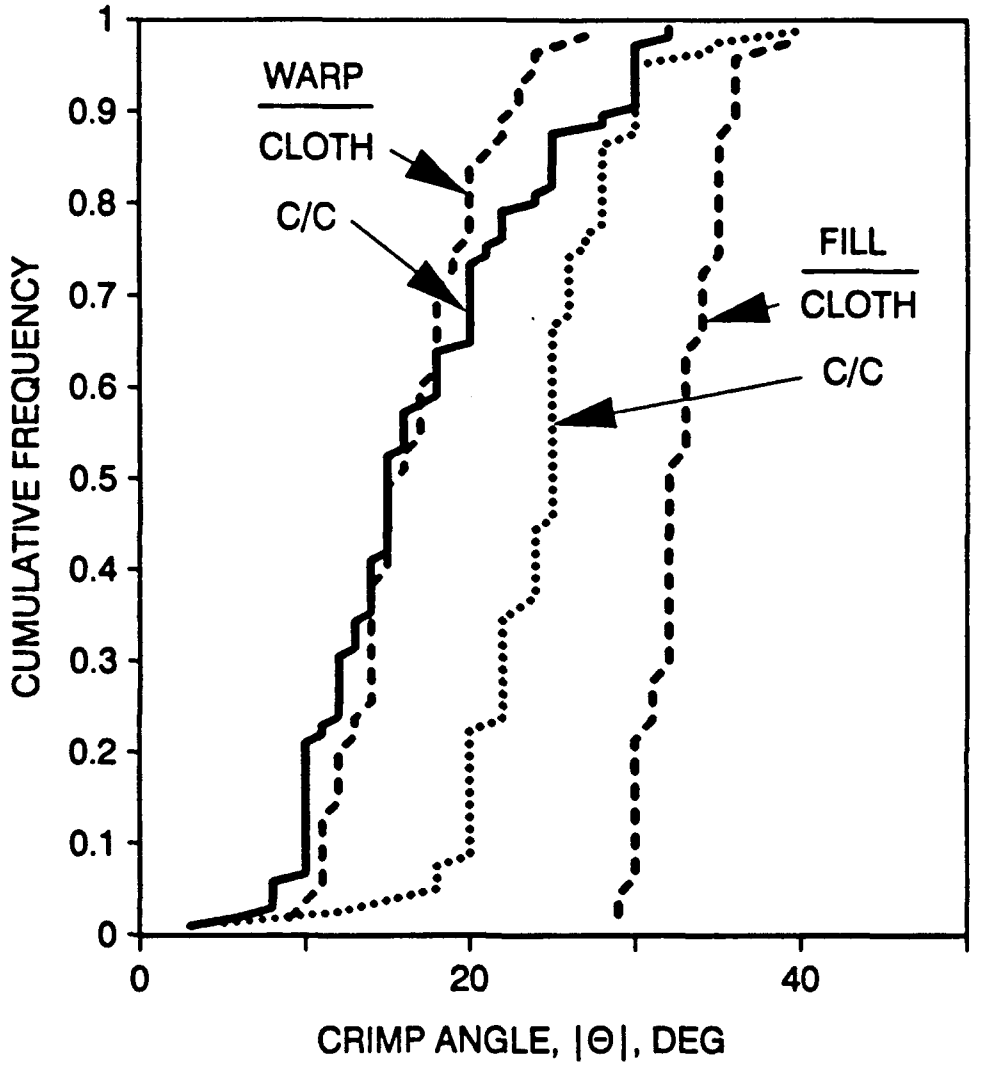

Fig. 5. Cumulative distributions of crimp angles measured in a fully-processed carbon-carbon panel (C/C), compared to crimp angles measured in the prepreg of Fig. 4.

wavelength. Crimp angles in warp yarns of the composite can range higher and lower than those in the prepreg; the increased variation of warp crimp angles appears caused by distortion of warp-yarn waveforms caused by lateral movement of individual fill yarns during compaction of the laminate.

Presumably, crimp-angle variations are essentially set when the matrix is cured; however, there should be a small general decrease in crimp-angle magnitudes as the laminate undergoes some crossply shrinkage during carbonization and graphitization [11].

2.4 Stacking Possibilities in Plain-Weave Laminates

Fig. 6 shows simplified two-dimensional representations of three stacking patterns in plain-weave-reinforced laminates. Usually, the pattern is oblique (Fig. 3, lower), but scattered zones of collimated stacking are also seen. When warp yarns of the cloth are collimated, the gaps between fill yarns (Fig. 3, upper) line up to form "walls" that are reinforced only with warp yarns. These matrix-rich walls are essentially unreinforced in the fill direction and, as Fig. 7 shows, contain larger microcracks than are seen in regions of oblique stacking. Fig. 8 is a detail view of such microcracking. Regions containing matrix-rich walls are likely to be of lower bulk density than regions of oblique stacking.

2.5 Stacking in Satin-Weave Laminates

Satin weaves are characterized by relatively long runs of nominally straight yarns; in an 8-harness weave these run across 7 crossing yarns; in a 5-harness weave they run across 4 yarn cross-sections. Therefore, nesting probably is not as important a factor as in plain (2-harness) weaves. There are essentially two stacking possibilities: the laminate may be laid up with each layer's warp yarns touching the neighboring layer's fill yarns, or the layers may be alternately flipped so warps are in contact with warps and fills with fills.

3. DEVELOPMENT OF MICROCRACKS

The results described below include observations using a hot stage in an optical microscope; several samples of 2D carbon-cloth-reinforced

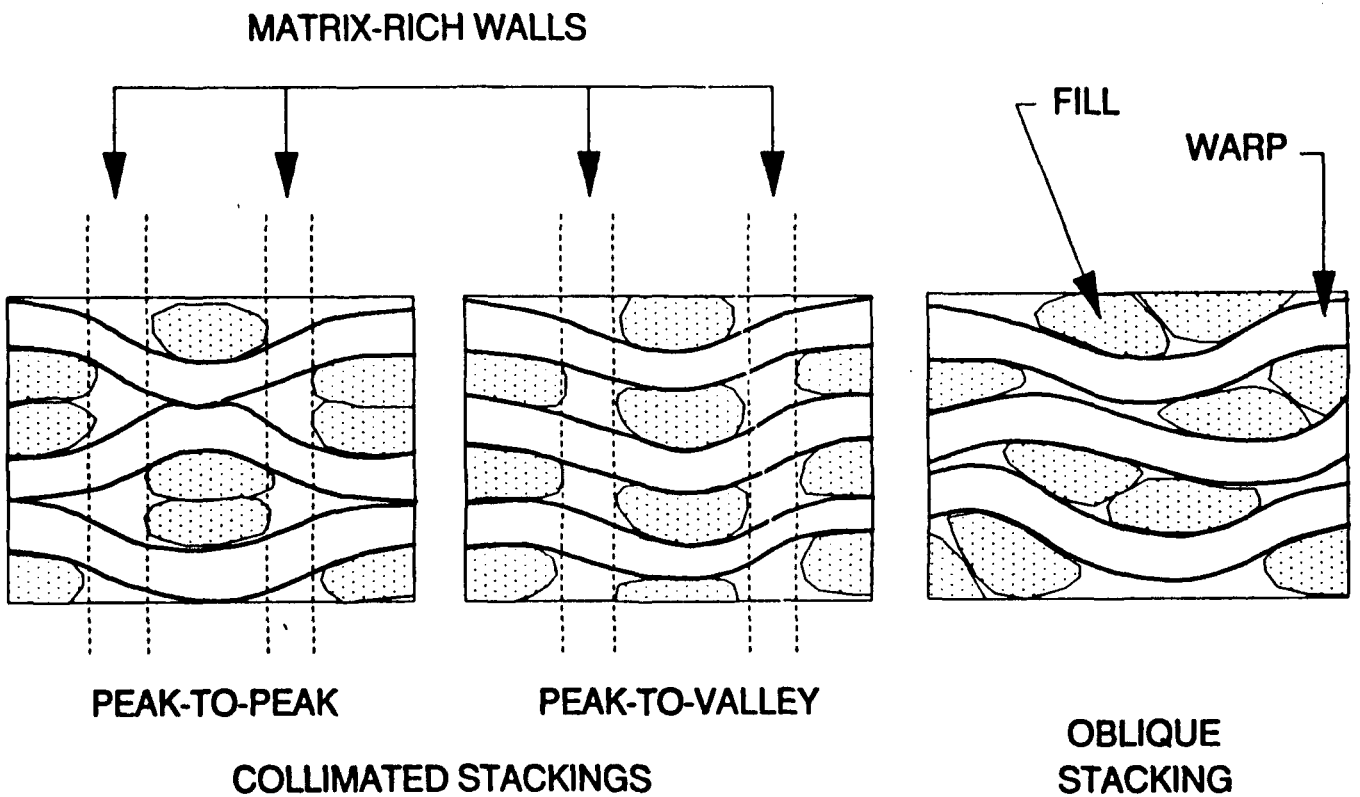

Fig. 6. Simplified two-dimensional descriptions of stacking possibilities for plain-weave laminates.

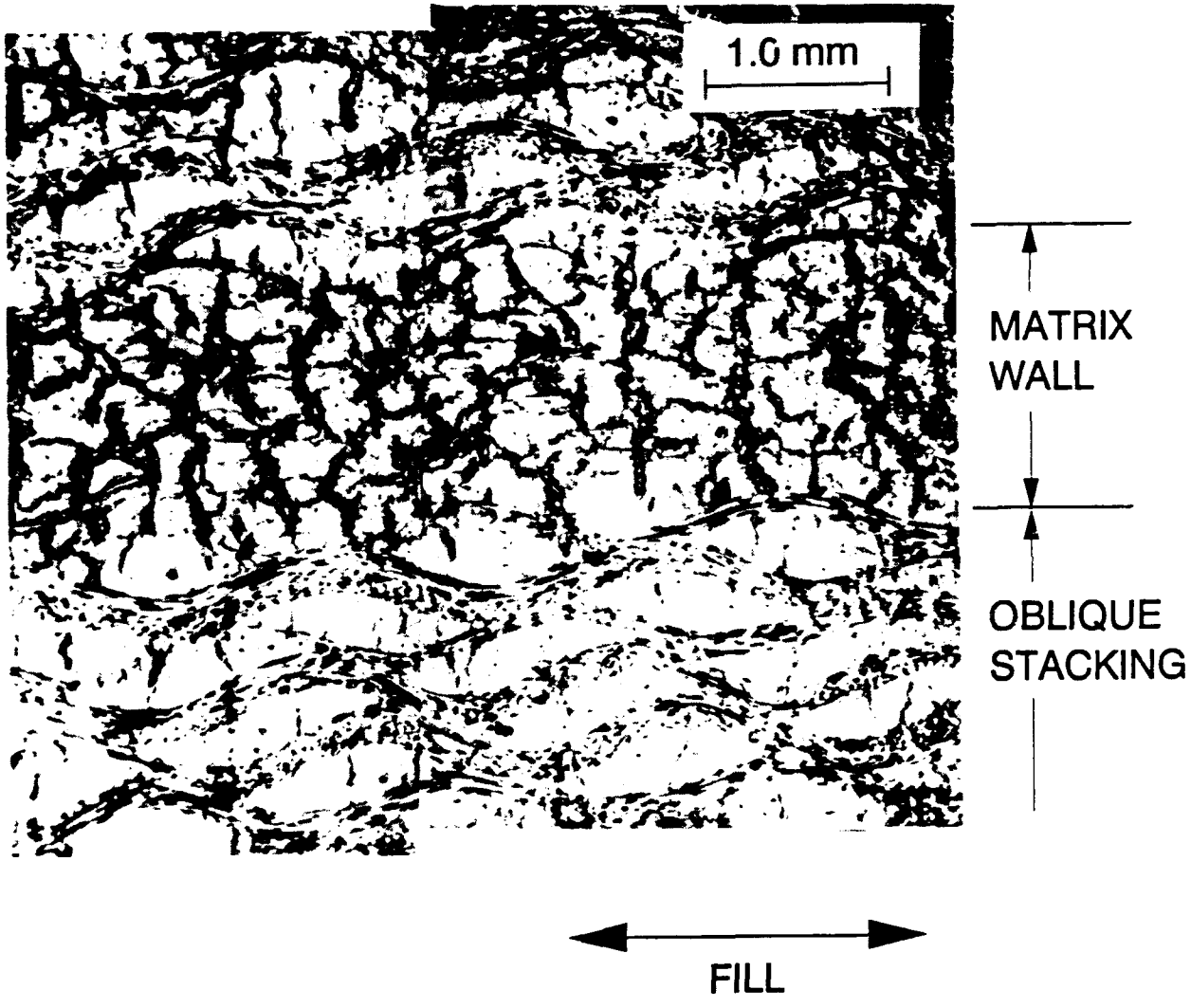

Fig. 7. Photomicrograph of a plain-weave reinforced carbon-carbon laminate showing excess cracking in matrix-wall region (see Fig. 6) compared to adjacent region of oblique stacking.

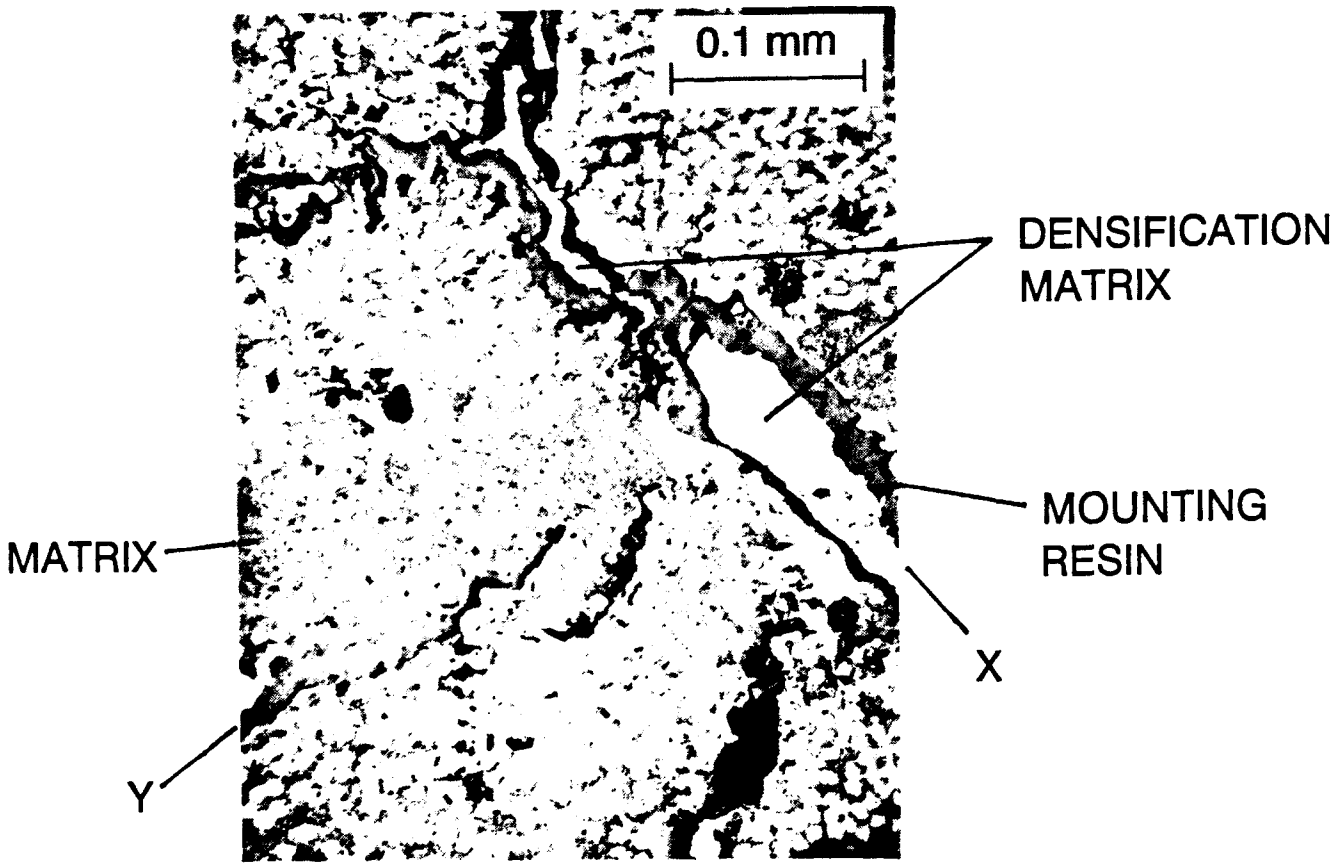

Fig. 8. Enlarged detail of matrix cracks in the matrix-wall region of Fig. 7; note the partial filling of one crack (X) with densification matrix and the apparent absence of such filling in crack (Y).

phenolic-resin-matrix laminates were observed between 20 and 580°C under flowing nitrogen [12]. The main purpose was to observe the formation and propagation of minimechanical microcracks during the first heating that carbonizes the cured prepreg resin in the compacted laminate. Photomicrographs of fully-processed laminates also are used to study changes in microcracking that occur during densification.

3.1 Hot-Stage Microscopy

Hot-stage observations for two phenolic-resin laminates are discussed:

a) Material A is a warp-aligned laminate of plain-woven WCA cloth. This material was prepared and studied by S. C. Brown of Aerojet, whose photomicrographs are used here (see also [12]).

b) Material B is a laminate of 8-harness satin-woven cloth of Thornel T-300 3K yarns; the yarns are made by Amoco [8].

Before heating in the hot stage, the panels had been cured to about 155°C in a pressurized autoclave. The specimens viewed were about 10-mm square on the viewing plane and about 3-mm thick. These dimensions approach the maxima the hot stage can accommodate. The viewing surfaces were prepared using normal metallographic wet-polishing procedures, but without any mounting resin. Photographs were taken through the microscope during heating and cooling.

The hot stage is a cylindrical copper block, insulated at sides and bottom, and heated with an electrical resistance cartridge inserted along the axis from the bottom. A shallow cavity centered at the top end contains the specimen; the cavity is covered with a glass slide and is purged with pure nitrogen, which is heated by its passage through a small-bore tunnel in the block. A thermocouple imbedded just below the specimen cavity provides temperature data and input signal to a programmable heater control. The microscope's objective is above the glass slide. Illumination is vertical through the objective. A layer of aluminum foil, with a sight hole, serves as a heat shield between hot stage and microscope; air is blown over the objective to keep it cool.

3.1.1 Strains and Cracking during Carbonization of a Plain-Weave Laminate

Fig. 9 shows Material A at 180°C (25°C above cure temperature) and at 510°C after heating at a uniform rate of 10°C per minute. The viewing direction is parallel to one set of yarns; the photos cover parts of two yarn cross-sections separated by a band of resin; individual fiber sections are readily seen in each bundle; the other yarns (out of the field of view on either side) run more or less parallel to the horizontal side of the photos. The distances marked on the top photo change during heating, as shown in Figures 10 and 11. The measurements, taken from enlarged photos, are estimated to be accurate to about ± .01 strain or about 2 μm crack width. The peak temperature reached was 580°C. Cooling was uncontrolled and quite rapid, initially more than 25°C per minute.

The following observations illustrate the complexity of local strain fields during carbonization:

a) Strain along "A" shows large shrinkage above 400°C, about the same magnitude as the linear shrinkage of phenolic resins heated without reinforcement. Inasmuch as "A" spans a resin band between yarn bundles, this is not surprising. The shrinkage continues during the initial cooldown, indicating the heating rate was too rapid to allow equilibrium of the carbonization reactions.

b) Strains along "D", however, are positive. "D" includes matrix, fibers, and the crack of width "B" (Fig. 11). When the crack width is subtracted from the measurements of "D", the strain, noted as "D-B" in Fig. 10 , is negative, indicating shrinkage of the fiber bundles as expected. The shrinkage of "D-B" is much less than of "A", presumably because fibers occupy much of the volume included in the measurement, and in rough agreement with measured crossply shrinkages of WCA/phenolic laminates during carbonization [11].

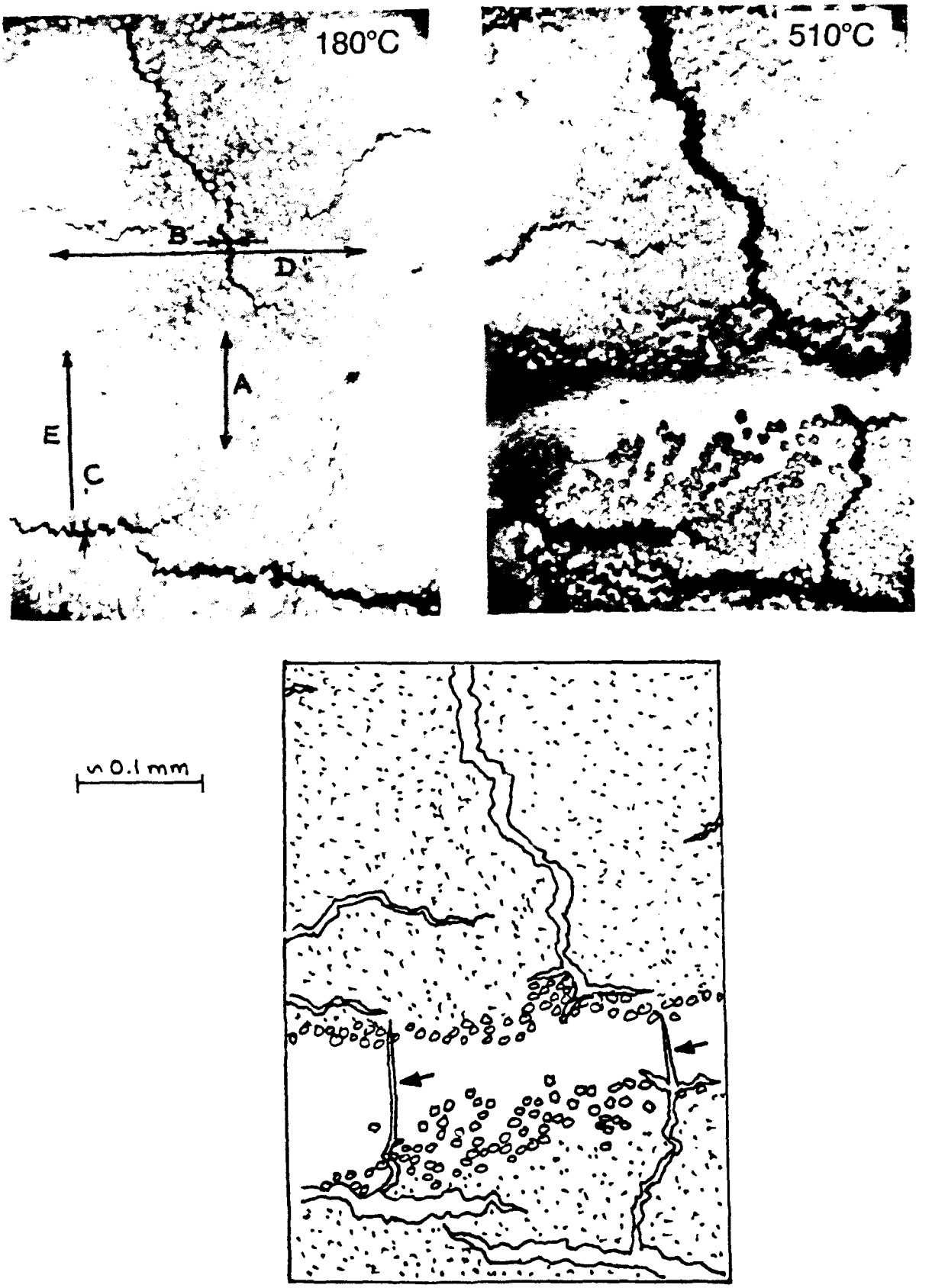

Fig. 9. Material A during heating. Photos, at 180°C and 510°C, by Scott C. Brown. Dimensions marked on 180°C photo are represented in Figures 10, 11 and 13. Shadows in the matrix band of the 510°C photo are due to distortion of the viewing plane because of matrix shrinkage. Arrows in the sketch show locations of new cracks that appeared in the matrix band on heating, between 540 and 580°C.

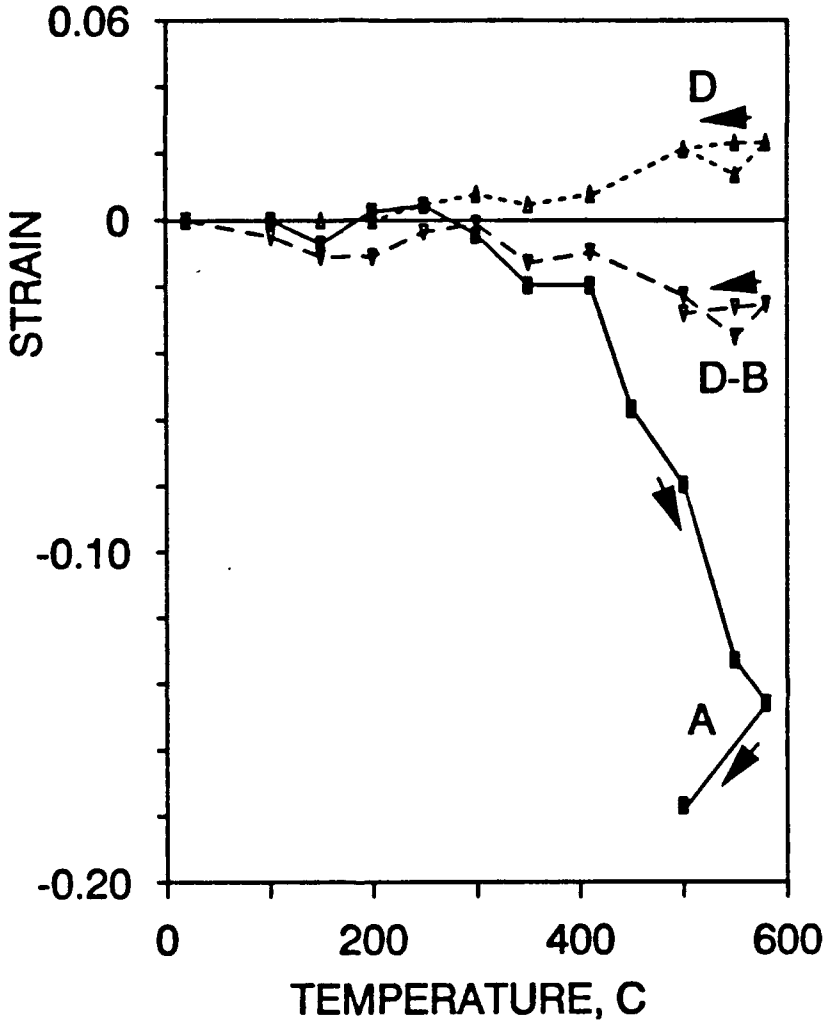

Fig. 10. Strains in Material A during heating.

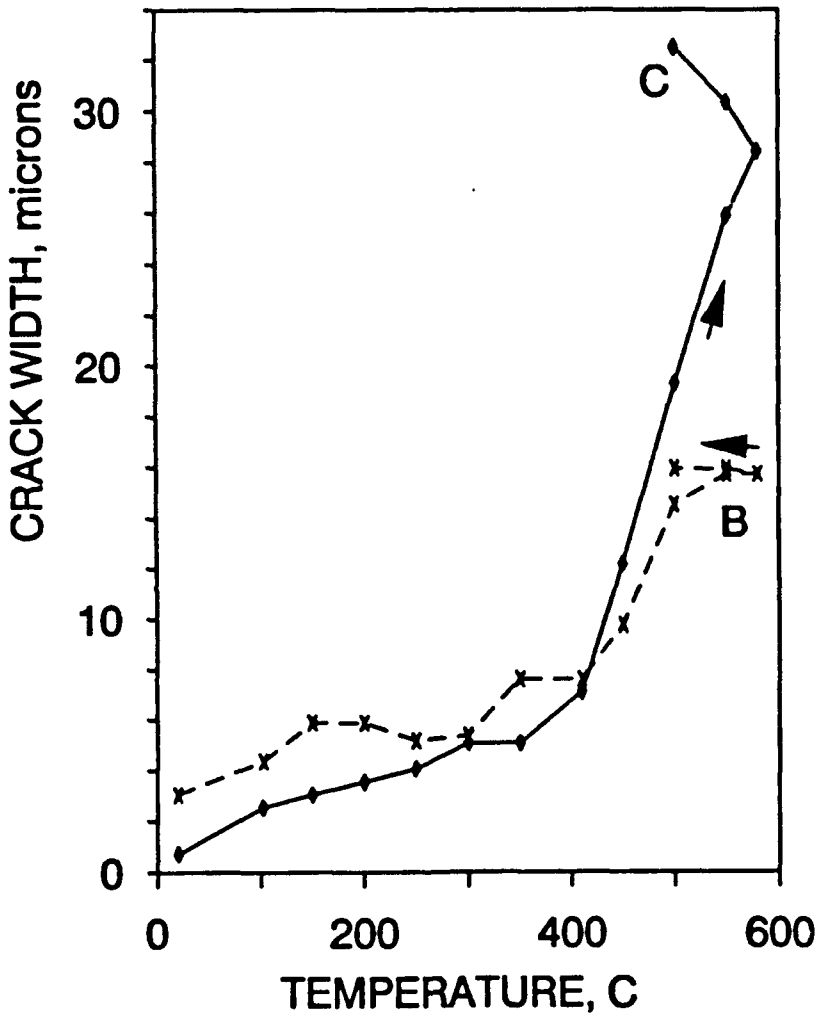

Fig. 11. Crack widths in Material A during heating.

c) Crack "C" (Fig. 11) widens rapidly above 400°C, becoming wider than "B" even though "B" and "C" were of similar width at the cure temperature.

The sketches in Fig. 12 show the inferred context of the region viewed in Fig. 9. The region is atypical because of the presence of the matrix band. The shrinkage of the matrix band in the crossply direction is accommodated by the opening of crack "C". Fig. 13 supports this statement by showing that the distance "E'" across the matrix band and the crack ($E' \approx E + C$) increases slightly during heating while the matrix-band width "E" decreases dramatically. The opening of cracks like "C", which run in the plane of the laminate, seems associated with such matrix bands. In the absence of the matrix band, the local crossply shrinkage presumably would be similar to that of the laminate as a whole, essentially equal to the shrinkage of fiber bundles.

The fact that cracks in the matrix band were not observed until temperatures above 530°C (Fig. 9) suggests the phenolic-based matrix is quite ductile at temperatures between 400 and about 500°C. Presumably, in this temperature range of intense chemical activity, the crossply shrinkage of the matrix band, accommodated by crack "C", allows the matrix to "flow" in the other direction without cracking. The large uniaxial strain probably is facilitated by the breaking and reforming of chemical bonds that accompanies pyrolysis.

3.1.2 Cracking in a Satin-Cloth Laminate

Fig. 14 shows Material B at room temperature after heating to 300°C at 10°C per minute with a 20-minute hold at 150°C and a 150-minute hold at 300°C. The yarns running within the plane of view are either warps or fills; the specimen was not marked as to these directions, but it is of small consequence as the satin weave is nearly balanced (nominally 23 fills and 24 warps per inch of cloth). The pattern of vertical cracks, of fairly regular spacing, is typical also of fully processed carbon-carbon laminates [13].

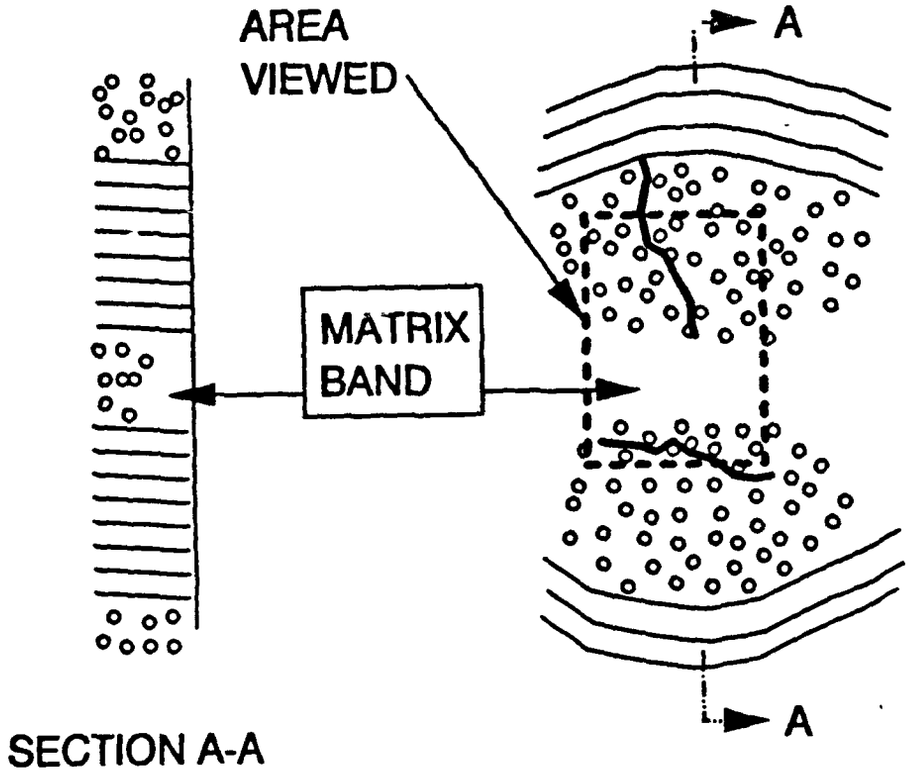

Fig. 12. Sketch of region surrounding that viewed in Fig. 9.

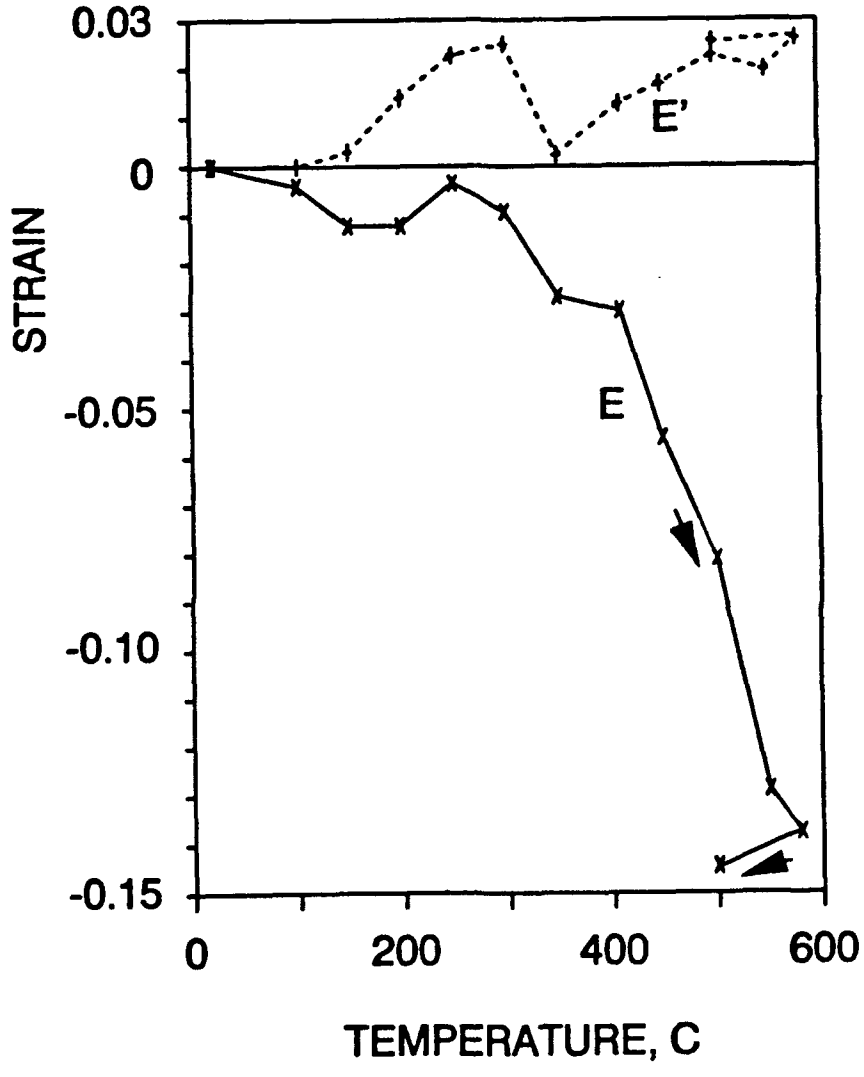

Fig. 13. Strains across matrix band in Material A.

Fig. 15 shows another specimen of Material B, viewed along the crossply direction at room temperature after cooling from heating to 434°C. The heating was at 10°C per minute with holds at 150°C for 60 minutes and at 430-434°C for 20 minutes. The aforementioned fiber-bundle cracks are seen here as lines parallel to the fibers. The matrix cracks marked "X" did not appear until the composite had reached 370°C; those marked "Y" were not observed until cooldown from the peak temperature of about 430°C. Thus, as in Material A, we see that the matrix pockets are more resistant to cracking than are the fiber bundles. The fact that these matrix cracks appear at temperatures lower than for the matrix band in Material A may be due to biaxial restraint (no cracks like "C" of Fig. 9 are seen in the vicinity of these smaller pockets).

Fig. 16 shows a third specimen of Material B after 2 minutes at 154°C (the cure temperature) and at 300 C during cooling from the peak temperature of 502°C. This specimen was heated at 10°C per minute with holds at 154°C for 26 minutes, at 300°C for 30 minutes, at 400 C for 26 minutes, and at 500-502°C for 20 minutes. The carbonization apparently induced some new cracks (indicated by arrows).

3.1.3 Remarks

Most of the cracks in both materials were visible at cure temperature, although they were narrower than after heating. The number of cracks seems greater after carbonization (Fig. 16), especially for Material B, but this inference needs verification with observations at higher magnification; the apparently new cracks may have been present as hairlines in the cured state. It is not yet clear whether the initial cracks were caused by resin shrinkage during cure, or by thermal stresses on cooling from the cure temperature; also, the degree to which initial cracks are affected by the polishing procedure has not yet been established.

For both materials, some changes in crack morphology were observed on heating of the cured specimens from room temperature to the cure temperature (about 150°C). These changes (apparently new cracks became visible and initial

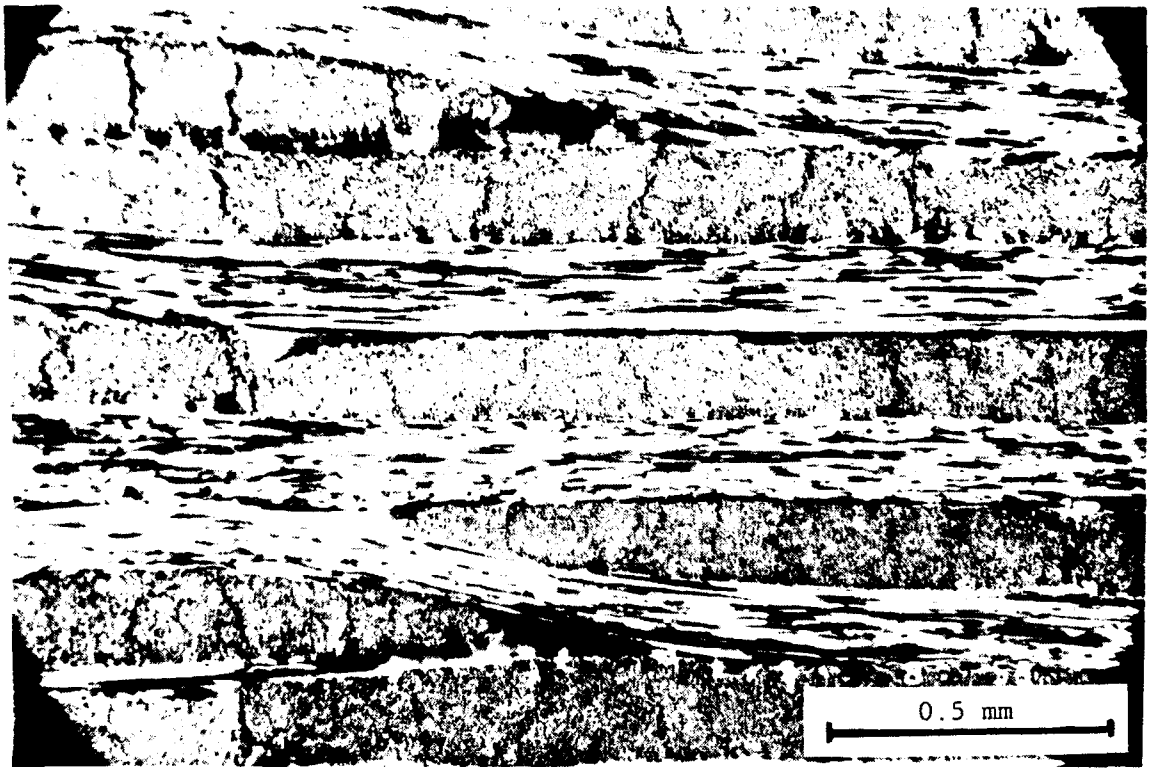

Fig. 14. Material B at room temperature after heating to 300°C.

Fig. 15. Material B at room temperature after heating to 430°C. The plane viewed is parallel to the plane of the laminate. X and Y denote new cracks in matrix (see text).

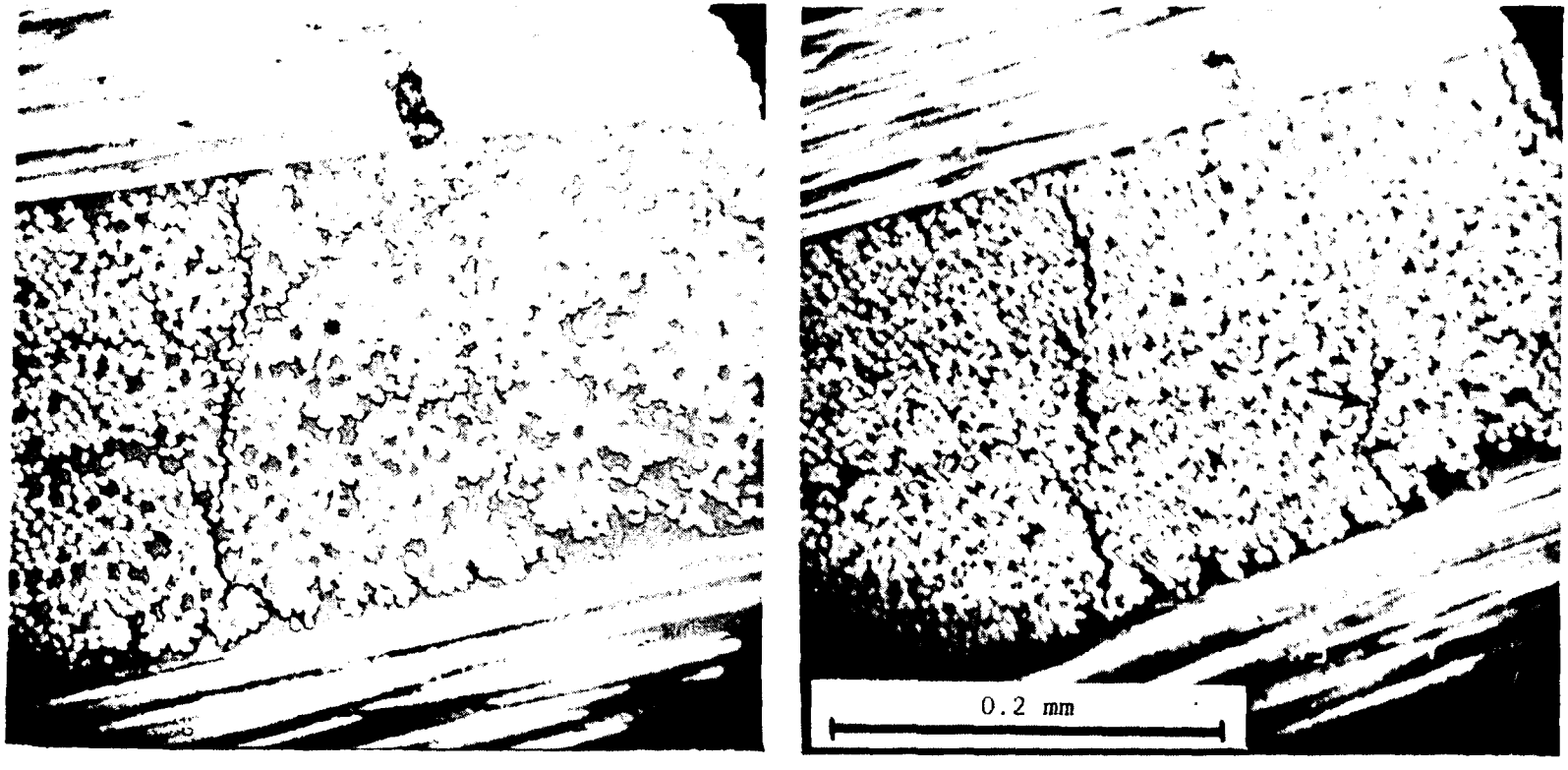

Fig. 16. Material B at 154°C (left) before further heating, and at 300°C after cooling from 500°C (right). Most cracks seen after heating to 500°C were visible at the cure temperature; the arrow points to what, at this magnification, appears to be a new crack.

cracks became wider) are assumed to result from matrix shrinkage caused by release of moisture that was absorbed during the wet-polishing. The effects of wet versus dry polishing procedures on microstructural appearance of cured specimens have not been studied.

For both materials, changes in crack morphology on cooling from 500-600°C were rather minor, suggesting that room temperature observations of cooled samples would be sufficient to capture most of the phenomena noted above. This finding is to be expected, considering that thermal-contraction strains on cooling are an order of magnitude smaller than the thermochemical-shrinkage strains on heating, and presumably would be more true of samples heated slowly enough to establish chemical equilibrium at each temperature.

The periodic cracks traversing the bundle cross-sections form two perpendicular arrays, corresponding to the warp and fill yarns. We may speculate that additional (delamination) cracks tend to form at the tips of the transverse cracks; these "shearlag" cracks, which are narrow and difficult to capture unambiguously on low-magnification photomicrographs, would allow the transverse-crack gaps to open without breaking fibers in neighboring yarns. The resulting crack network forms an interconnected space (Fig. 17), which may be the primary path by which densifying liquids penetrate the laminate.

3.2 Crack Spacings

Several carbon-carbon laminates were examined microstructurally by Carroll [14] after cure of the prepreg resin, after the first carbonization, and after densification (with a final graphitization). To study the development of minimechanical cracks that traverse fiber bundles (Fig. 17), measurements of crack length and spacing were made from Carroll's photomicrographs at 20X magnification. Photos of one material were examined; the laminate was reinforced with 5-harness cloth of Thornel 300 yarns prepregged with a phenolic resin.

Results are presented in Fig. 18, in terms of the ratio of spacing between two neighboring cracks to the length of one of the two cracks. At all stages of

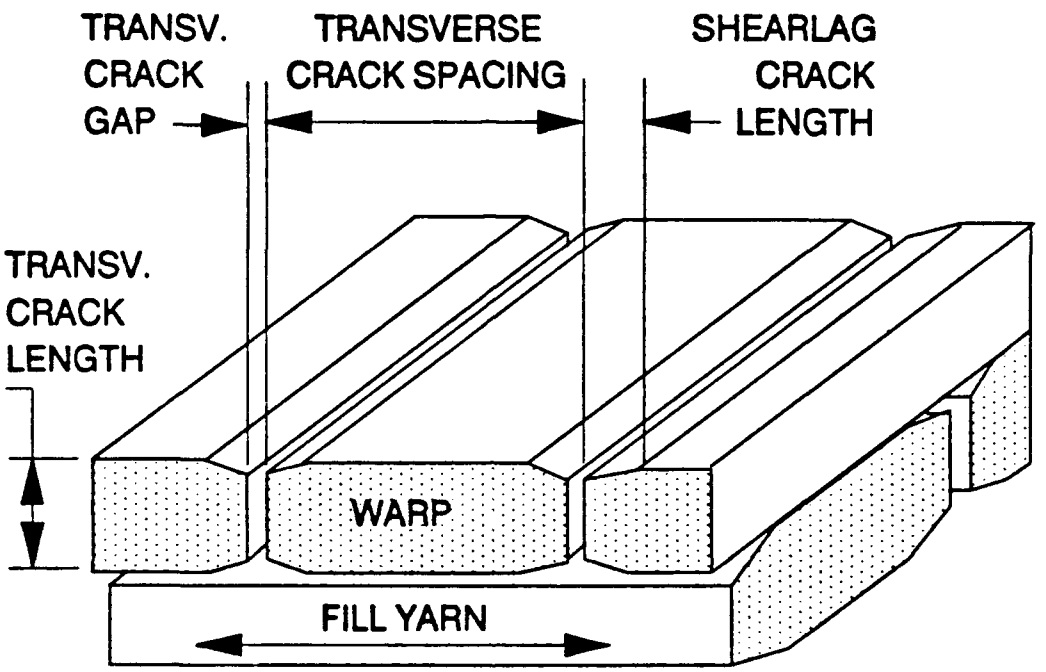

Fig. 17. Sketch of periodic cracking across fiber bundles.

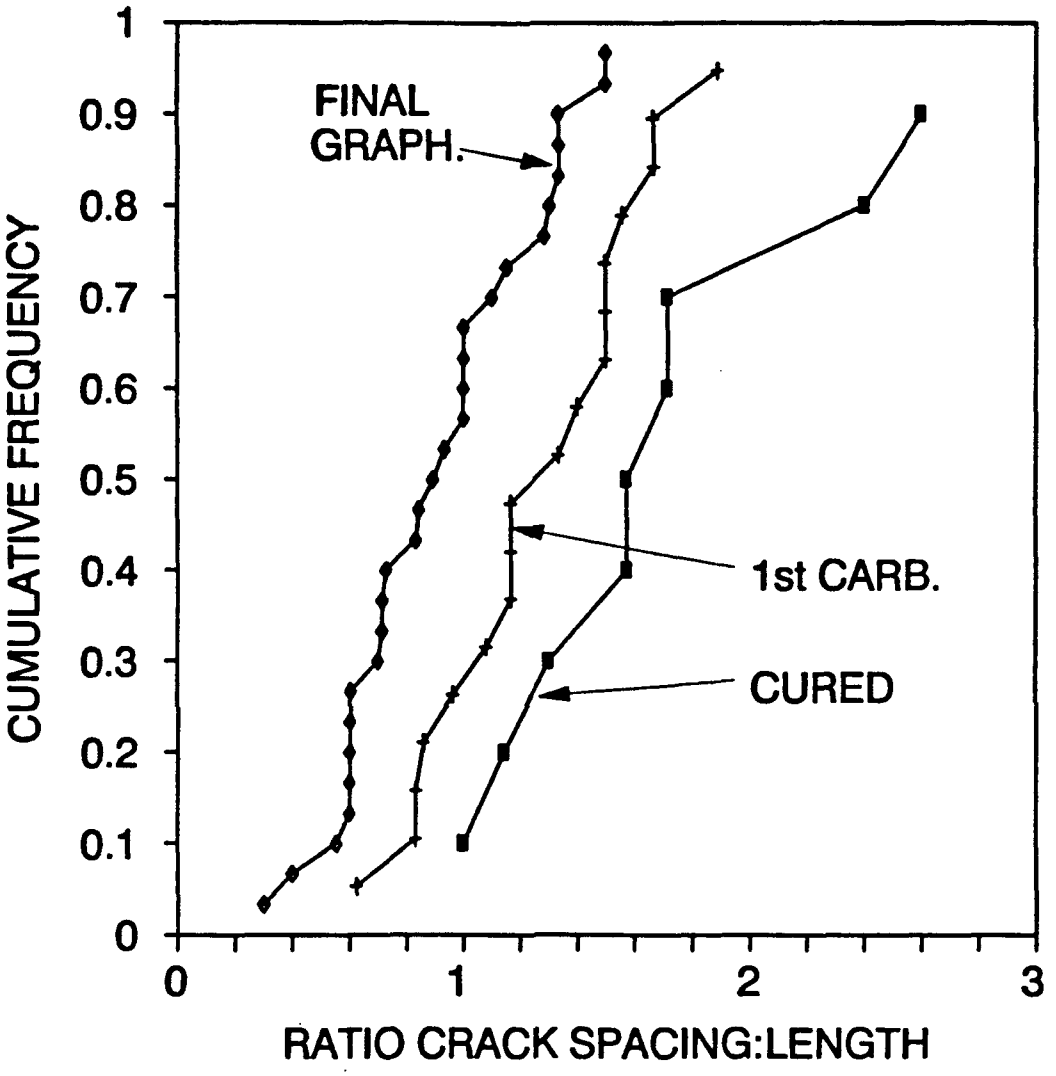

Fig. 18. Crack spacing distributions in T-300 5-harness laminates made with phenolic prepreg, measured from photos from Carroll [14].

processing, the crack lengths are essentially equal to local crossply distance between the fiber bundles. In this laminate, there is a clear progression toward smaller crack spacings (more numerous cracks) as processing proceeds, and, there is considerable variability in length-spacing ratios. A more comprehensive examination would be needed to explore the variability further. Also worth pursuing would be measurements of crack gaps to study the void volume associated with the minimechanical cracks, and measurements of the lengths of any associated delamination cracks (Fig. 17).

4. CONCLUDING REMARKS

Although microstructure is widely acknowledged to be a primary determinant of engineering properties of composites, relatively little quantification of microstructural features has been attempted for carbon-carbon laminates, perhaps because their microstructure is perceived to be quite complex. Prior work seems limited to some characterization of fiber-matrix interface regions [7] and some exploratory study of crimp angles [3,4]. This paper demonstrates that informative statistics can be obtained from various rather simple measurements at a minimechanical level. More work along these lines seems warranted to support the development of realistic models of composite behavior.

The study so far has shown:

a) Crimp angles of the yarns in one plain-weave carbon cloth are quite variable and are significantly affected by compaction of the laminate; crimp angles of fill yarns appear decreased by compaction, whereas the crimp angles of warp yarns seem little affected on average but their variance was increased by the lateral movement of fill yarns during compaction.

b) Most of the microcracks traversing fiber bundles in the carbon-carbons, reinforced with plain-weave or satin-weave cloths, were present after cure of the resin-prepregged laminate; the number of cracks increases during further processing and the crack gaps widen. Most of the open cracks run across fiber

bundles in the crossply direction (without breaking fibers); however, in the plain-weave laminate, open cracks also occur in the plane of the laminate in regions of collimated stacking.

c) Pockets of unreinforced phenolic matrix within the laminate are more resistant to microcracking during heat treatment than are the phenolic-impregnated fiber bundles. The linear shrinkage of in-situ resin pockets during carbonization, when unrestrained by virtue of the opening of cracks in neighboring fiber bundles, appears similar in magnitude (15 to 20 percent) to the shrinkage of neat resin. The linear strain capability of the phenolic matrix, before it cracks, is inferred to be surprisingly large (about 15 percent) at temperatures between 400 and 500°C, when the matrix is relatively unrestrained in the two perpendicular directions.

The quantitative information presented here was obtained by manual measurements of microstructural features. As the manual process is somewhat tedious and expensive in terms of labor, the number of measurements has not been sufficient to establish the statistical significance of the various inferences. Computer-aided image-analysis would be useful for gathering larger amounts of such data.

Acknowledgments

This work was sponsored by the Office of Naval Research under contract N00014-82-C-0405; a discussion with Dr. L. H. Peebles, Jr., ONR's Scientific Officer, stimulated some of the interpretation of hot-stage observations. Mr. H. O. Davis of Kaiser Aerotech supplied a sample of prepregged WCA cloth. Mr. Scott C. Brown of the Aerojet Strategic Propulsion Company made available his original photomicrographs of a plain-weave laminate undergoing heating in a microscope hot stage. A sample of as-cured laminate reinforced with 8-harness T-300 cloth was supplied by Dr. James Sheehan of General Atomics. Discussions with Professor Steven Yurgartis of Clarkson University, who is collaborating in the ONR-sponsored research by developing computer-aided image-analysis techniques for characterizing yarn crimp and nesting, were a beneficial influence. The Aerospace Corporation, via Dr. Gerald Rellick, made available their hot-stage microscope facility for some of this work; the hot stage was developed by Mr. Manfred Buechler: Mr. Pat Sheaffer of Aerospace Corp. assisted the author in operation of the hot-stage. The author is grateful to these individuals and organizations for their support and cooperation.

REFERENCES

1. T. Ishikawa and T-W. Chou, *J. Comp. Mat.*, 17, pp. 399-413 (1983).
2. J. Jortner, in *Advances in Composite Materials and Structures* (S. S. Wang and Y. D. S. Rajapakse, Editors), AMD-Vol.82, American Society of Mechanical Engineers, pp. 135-146 (1989).
3. J. Jortner, in *Symp. on High Temperature Composites, Proc. of the American Society for Composites*, Technomic Publishing Co, pp. 243-251 (1989).
4. P. B. Pollock, *Carbon*, 28, pp. 717-732 (1990).
5. J. Jortner, *Carbon*, 24, pp. 603-613 (1986).
6. L. H. Peebles, Jr., R. A. Meyer, and J. Jortner, in *Interfaces in Polymer, Ceramic, and Metal Matrix Composites* (H. Ishida, Ed.), Elsevier, pp. 1-16 (1988).
7. R. A. Meyer, in *Ext. Abstr. of the 19th Biennial Conf. on Carbon*, American Carbon Society, pp. 334-335 (1989).
8. D. J. Renzo (Editor), *Advanced Composite Materials - Products and Manufacturers*, Noyes Data Corp, pp. 768-781, (1988).
9. J. Jortner, A. A. Kelton, P. C. Hopkins, In-Situ Densities of Fibers and Matrices in Carbon-Carbon Composites, Report MCD-G7385, McDonnell-Douglas Astronautics Company, (May 1978).
10. F. Albugues, Y. Grenie, and M. Villatte, in *Ext. Abstr. of 16th Biennial Conf. on Carbon*, American Carbon Society, pp. 492-493 (1983).
11. K. Marnoch, Presentation to Symp. on Carbon Fibers and Composites, American Carbon Society, Buffalo, July 1988.
12. J. Jortner and S. C. Brown, in *Ext. Abstr. of 19th Biennial Conf. on Carbon*, American Carbon Society, pp. 350-351 (1989).
13. B. A. Ford, R. G. Cooke, and B. Harris, in *Ext. Abstr. of 17th Biennial Conf. on Carbon*, American Carbon Society, pp. 233-234 (1985).
14. H. B. Carroll, unpublished work, Hercules Aerospace Co. (1986).

CHAPTER 2

NOMENCLATURE FOR YARN SHAPES

A tentative taxonomy is offered for description of yarn waveforms. Figures 1 and 2 illustrate some of the concepts. Implicitly it is assumed that we are looking at a section of a warp-aligned laminate; the observed plane contains the crossply vector and a line parallel to a yarn direction (warp or fill).

x. Coordinate along a line parallel to the plane of the laminate (and in the plane of view).

y. Coordinate perpendicular to x (and in the plane of view).

WAVE or WAVEFORM. The curved line representing the direction of fibers, projected onto the viewing plane, in a yarn that is oriented generally in the x direction.

UPPER WAVE. The wave representing the boundary of the yarn, in the viewing plane, at which y is greatest.

LOWER WAVE. The wave representing the boundary of the yarn, in the viewing plane, at which y is least.

CENTER WAVE. The wave representing the centerline of the yarn, as seen on the viewing plane. Tentatively, the centerline is defined as the line through the y points representing the average of the upper-boundary y and the lower-boundary y at each x.

PEAK POINT. A point on the wave where y reaches a local maximum.

TROUGH POINT. A point on the wave where y reaches a local minimum.

RAMP. That portion of a wave between a trough point and a neighboring peak point.

POSITIVE RAMP. A ramp between a trough point and the peak point to its right.

NEGATIVE RAMP. A ramp between a peak point and the trough point to its right.

RAMP AMPLITUDE. The y distance between the trough and peak points that bound the ramp.

RAMP LENGTH. The x dimension of a ramp.

RAMP ANGLE. The angle whose tangent is $(y_R - y_L)/(x_R - x_L)$, where the subscripts R and L represent the right and left boundaries of the ramp.

WAVELENGTH. The x distance between two nearest trough points, or between two nearest peak points.

INCLINATION ANGLE. The angle between the tangent to the wave and the x axis, at any x location.

CRIMP ANGLE. Angle of greatest inclination within a single ramp. More precisely, the inclination angle at the point within a ramp at which the absolute value of inclination angle is a maximum. Crimp angles may be positive or negative.

AVERAGE CRIMP ANGLE. The average of the absolute values of crimp angles for some set of neighboring ramps in the laminate.

AVERAGE CRIMP ANGLE OF A YARN. The average crimp angle for a set of ramps along a single yarn. The number of positive and negative ramps sampled should be equal.

AVERAGE CRIMP ANGLE FOR A LAMINATE. The average crimp angle for a set of ramps representing each yarn in the viewing plane of a laminate; preferably, the same number of ramps should be sampled in each yarn.

CROSSING LINE. A line in the viewing plane that is parallel to the y direction.

CROSSING ANGLE. The inclination angle at the point where the wave intersects the crossing line.

CROSSING-ANGLE DISTRIBUTION. Refers to the inclination angles of waves representing several neighboring yarns where each wave intersects the same crossing line.

INCLINATION-ANGLE DISTRIBUTION. Refers to the inclination angles measured on one or more waves at equally spaced values of x, such that $\Delta x \ll$ wavelength, over a total x-distance that comprises an integral number of wavelengths of one of the waves included in the sample.

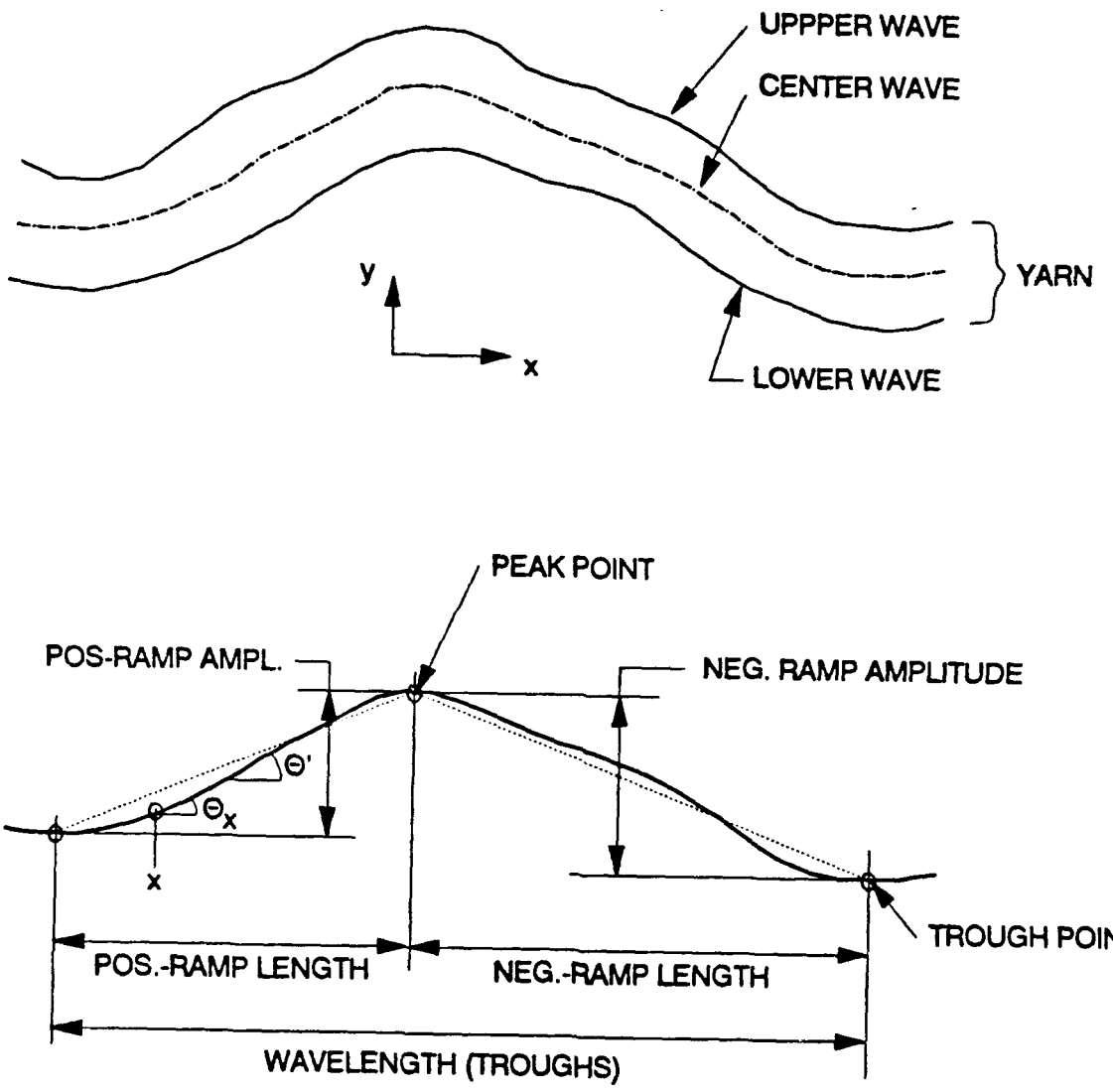

Fig. 1. Nomenclature for description of yarn waves (tentative).

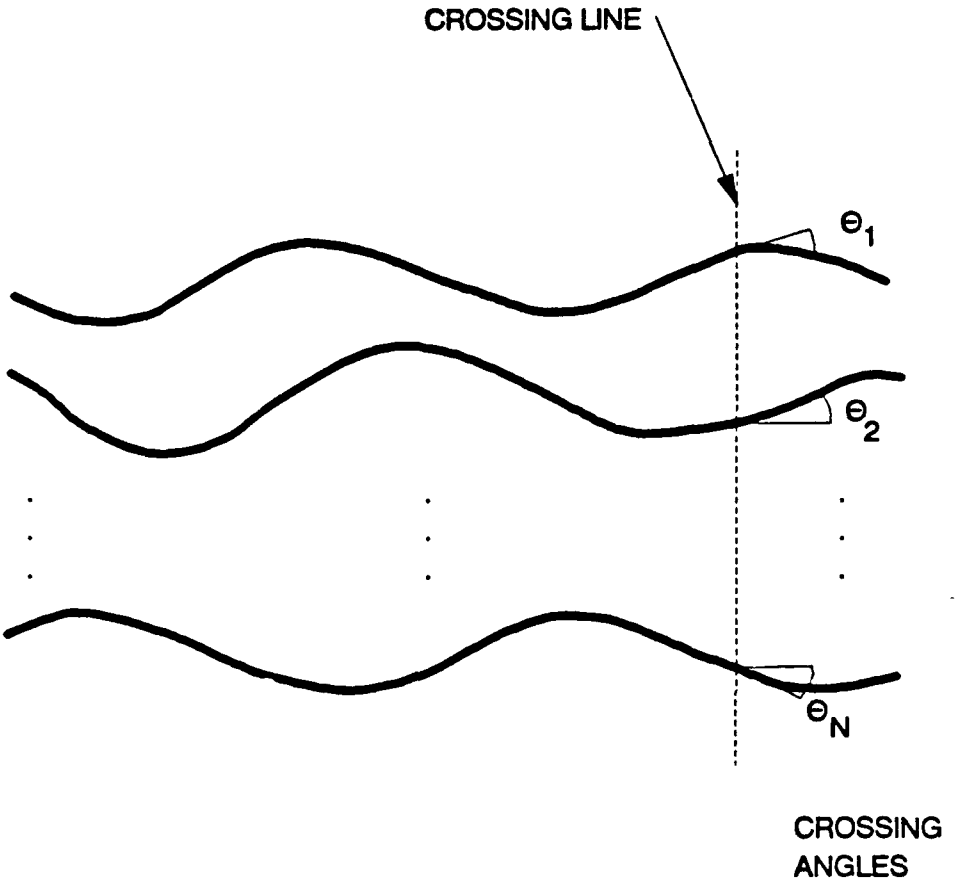

Fig. 2. Crossing line and crossing angles.

REMARKS

Of the distributions defined above, the most general for modeling probably would be the inclination-angle distribution taken over the full thickness of the laminate; that distribution would represent the laminate (or a test specimen thereof), because it approximates the distribution of fiber-orientation angles for elements of equal volume.

The crossing-angle distribution, when taken over the full laminate thickness, also is appealing for modeling of response to loadings in the yarn direction, because it may be taken to represent the inclination angle distribution of one "slice" of the laminate. The variation of crossing-angle distributions along the length of the laminate can be interpreted (in a 2D analysis) as related to the variability of properties.

Crimp angles of the yarn centerlines seemed the obvious thing to estimate manually [1], and their average is a convenient summary number. But they don't give any information about how much material is represented by each crimp angle. A better representation (yet to be explored) might be a mean of crimp angles weighted with their respective ramp lengths.

The center wave is the one to look at, rather than the upper and lower boundary waves. The yarn boundaries in the viewing plane are affected by the local shape of the yarn's cross-section; probably, the inclination angles at the boundaries do not represent much material and their extreme values probably are not of much significance.

Ramp statistics may prove useful. Ramp angles may be an alternate measure of shape, one that bypasses many of the extreme angles picked up in the other distributions. Measuring ramp amplitudes, lengths, and angles, might prove useful for the sake of evaluating these measures for use in models and as a intuitively accessible way of checking the meaning of the other angular measures.

REFERENCES

1. J. Jortner, "Effects of Crimp Angle on the Tensile Strength of a Carbon-Carbon Laminate," in *Symp. on High Temperature Composites, Proc. of the American Society for Composites*, Technomic Publishing Co, pp. 243-251 (1989).

CHAPTER 3

MEASUREMENT OF YARN SHAPE AND NESTING IN PLAIN-WEAVE COMPOSITES

The following paper (to be submitted for publication) summarizes efforts at Clarkson University to apply computer-aided image-analysis techniques to the measurement of yarn geometries in plain-weave laminates.

Measurement of Yarn Shape and Nesting in Plain—Weave Composites

S.W. Yurgartis, K. Morey
Clarkson University

J. Jortner
Jortner Research and Engineering, Inc.

1 Introduction

Composites reinforced with layers of woven cloth have a distinctive morphology in that the yarns (fiber bundles) comprising the cloth follow wavy paths as they pass over and under each other (eg, Figure 1). The strong dependence of composite properties on fiber orientation implies that geometry of the wavy path ("yarn shape") is an important feature of these materials. Also important is the degree to which adjacent yarn waves are in phase, a function of the "nesting" of cloth layers in a composite laminate. Yet, for lack of detailed morphological studies of real materials, current analyses of cloth-reinforced laminates assume highly simplified idealizations of yarn shapes and, frequently, ignore entirely the question of nesting. The purposes of this paper are to: 1) propose some quantifiable measures of yarn shape and nesting; 2) describe the use of digital image analysis to acquire statistical distributions of these measures; and 3) present and discuss some examples of yarn-shape and nesting data. The work is part of a larger effort to develop quantitative links between microstructure and properties in cloth-reinforced composite materials. This initial effort deals primarily with laminates of plain-weave cloth.

2 Background

The study of yarn shape began, naturally, with textiles. Although textile models are not directly related to composite behavior because usually they treat only one layer of cloth and omit consideration of a matrix, they do serve to identify potentially important descriptors of yarn shape. Hearle, Grosberg, and Backer [1] provide an extensive review of textile mechanics and deal in detail with the effects of yarn shape. Pierce [2] introduced much of the terminology used to describe yarn shape, and provided a basic model of woven fabrics. Olofsson [3] and Kawabata [4], among others, have modeled the stress-strain behavior of fabrics in terms of yarn-shape parameters, such as crimp angle, wavelength, and wave amplitude. In the absence of a matrix, load-deflection behavior is nonlinear and anisotropic because yarn shape changes with extension. Similar nonlinearities occur in "flexible" composites, comprising a fabric in an elastomeric matrix (cf, Stubbs [5] and Chou [6]).

Experimental comparisons between woven and non-woven reinforced composites have been made by Bishop [7], who compares mechanical properties of carbon/epoxy laminates made with cloth (a 5-harness-satin weave) to those made with the same fiber in unidirectional plies laid up at right angles. After accounting for differences in fiber-volume fractions, Bishop's data show the woven laminates to have substantially lower tensile and compressive strengths (and stiffnesses) when loaded parallel to a set of fibers, greater sensitivity to notches, and less damage after equivalent impacts; she attributes these effects to "fiber distortion" (or yarn shape) in the woven composites.

Some of these results are, at least qualitatively, explained by several available models that account for yarn shape, as discussed below.

Early models for the effects of reinforcement undulations on elastic properties of composites, reviewed by Jortner [8], deal explicitly with wrinkle anomalies in nominally straight-fiber composites but are, in principle, adaptable to the analysis of woven materials; the analytical models usually treat only simple yarn shapes (like sinusoids), but some of the numerical models can treat arbitrary yarn shapes. The potential significance of nesting (as represented by phase relationships among yarns in neighboring cloth layers in a laminate) may be deduced from the large differences between properties predicted assuming all yarn undulations are in phase and those predicted assuming random nesting ([6][8]).

Chou and Ishikawa [9] describe several models for analyzing the stiffness and strength properties of cloth-reinforced composites. When yarn undulations are accounted for explicitly, as in their "crimp" (or "fiber undulation") model, the waveforms are taken as sinusoidal. These models are said to predict the major effects of weave style (plain-weave versus satin weaves of various harness numbers) reasonably well for some graphite/epoxy composites, although experimental confirmation seems quite sparse, and some of the validation is in the form of comparisons to finite-element analyses of similar geometries.

Finite-element modeling of the unit cells of cloth-reinforced composite is of continuing interest (eg,[10]). Whitcomb's [11] treatment of plain-weave composites, perhaps the most ambitious attempt so far, includes 3D elastic analysis of the three-dimensional geometry of interwoven yarns for one nesting configuration. Commenting on the strain gradients predicted within yarns of a stressed laminate, and their relevance to predicting damage in woven materials, Whitcomb notes that "some of the most severe strain gradients occur where the weave geometry is most difficult to model with confidence", and calls for experimental work to "characterize the variation of fiber tow geometry."

Nonlinear stress-strain responses observed on loading of some brittle-matrix laminates have been explained in terms of localized tensile damage and modeled by considering the anisotropy of strength of yarn bundles (they are much weaker in transverse tension than in axial tension) in combination with weave-related yarn shapes (eg, Chou and Ishikawa [9] and Jortner [12]).

Details of yarn shape appear especially significant for composites made with yarn bundles that exhibit large ratios of axial stiffness to shear stiffness, such as certain carbon-carbon composites; some carbon-carbon yarn bundles are so anisotropic that nonlinear geometric effects (such as strain-induced changes in fiber orientation, normally considered only at large strains in "flexible" composites) become important even at small strains [13][12].

Jortner [14] found that much of the wide scatter observed in the tensile strengths of ostensibly similar carbon-carbon laminates, all reinforced with plain-weave cloth, could be related to uncontrolled variations of crimp angles of the loaded set of yarns; he found the average load per load-bearing yarn at tensile failure of the composite to be inversely proportional to the sine of the average of the crimp angles measured on the test specimen. Pollock [15] studied similar plain-weave composites and derived Jortner's correlative equation by analyzing the bending of a wavy yarn subjected to a tensile load. Correcting for average crimp angle does not remove all scatter in tensile strengths; Pollock suggests the remaining scatter (that is not attributable to variability of fiber properties) may be related to the variance of the crimp-angle distribution in a tensile specimen. From observations of fracture surfaces, Pollock speculates that the path of fracture across the laminate is influenced by the nesting of adjacent cloth layers.

With the exception of the crimp-angle data mentioned above, few measurements are available of

Figure 1: Example of yarn shape in a carbon-carbon composite reinforced with a plain weave cloth. The fibers appear lighter in color. This is a micrograph of the fill yarns of Panel A, as discussed in the text.

actual yarn shapes in cloth-reinforced laminates. Analysts have relied on idealized definitions of yarn shape, chiefly sinusoids, with wavelengths and amplitudes determined from a knowledge of the cloth weave plan and, perhaps, the average ply thickness in the laminate. The problem of determining the numerical inputs that describe yarn shape for a specific laminate is not usually discussed (eg, [9][12]). Actual yarn shapes are not necessarily simply related to descriptors of the cloth weave. Jortner [16] notes that across-ply compaction during lamination of a plain-weave composite, while it does not significantly change the weave's wavelengths (yarn spacings), can substantially affect crimp angles and distort wave forms; that yarn shapes can vary within a laminate and that statistical distributions, rather than deterministic values, are needed to describe them; and that nesting patterns also can be quite variable and complex.

3 Measures of Yarn Shape and Nesting

In light of the known and suspected influences of yarn morphology on composite properties, and the need for model input data, a effort was undertaken to develop quantitative measures of yarn shape. Two measures of yarn shape itself and one measure of the way adjacent cloth layers nest are chosen for initial development. These measures are illustrated in Figure 2 and described below.

Inclination angle is the angle between the tangent of the yarn axis and the mean yarn direction. The distribution of inclination angles gives a statistical representation of yarn shape with respect to orientation.

Crimp angle is the maximum absolute value of inclination angle between a yarn-wave peak and trough. If the wave form of the yarns is known or assumed to be sinusoidal, the crimp angle can be one of two fundamental parameters that fully define shape (the other being amplitude or wavelength). Also, as it represents the extremes of reinforcement deviation from the lamination plane, the crimp angle may be expected to influence strength and stiffness.

Angle match is the absolute value of the difference between inclination angles of adjacent yarns. If yarns were periodic and uniform in shape, angle match measurements would be a way to characterize the phase match between adjacent yarns. An advantage to using-angle match, rather than another measure such as phase angle, is that a periodic yarn shape is not required for it to be meaningful.

The techniques used to make these measurements also can provide data for yarn-volume fraction and a best-fit sinusoidal approximation to yarn shape.

Measures of other potentially important morphological characteristics, such as yarn-bundle twist, fiber distribution within bundles, and yarn cross-sectional shape, are not addressed here.

4 Application of Digital Image Processing

A goal of this work was to automate yarn shape measurement as much as possible using digital image processing. The statistical nature of microstructural measurements makes large sample sizes desirable, and when coupled with the complexity of the microstructure, the use of computer-aided image processing is very attractive. The rapidly improving power and decreasing cost of image processing equipment is making this approach increasingly feasible and available for routine application.

Equipment for the present work consisted of a Sun 3/260 workstation computer as host to

Imaging Technology 150 Series image processing hardware. The image processing capabilities of this system are substantially greater than current PB-based systems. Images were photographed with a high resolution Dage-MTI NC70 video camera attached to an Olympus PME reflected light optical microscope. Digitized pictures were 512 x 512 pixels, with 256 gray levels. Software to analyze the images was written in-house; about 1450 lines of C-code were needed to accomplish the image processing tasks.

4.1 Two-Stage Measurement Process

The measurement of the distributions of inclination angle, crimp angle, and angle-match proceeds in two stages: 1) identifying the yarn boundaries and fitting a function to match the boundaries, and 2) extracting information from the yarn boundary data. The technique is illustrated here with data collected from plain-weave carbon-carbon composites. It should be readily adaptable to other composite systems.

4.2 Functional Fits to Yarn Boundaries

A semi-automatic method was developed for the initial stage of identifying yarn boundaries. Random, non-overlapping views of polished sections of a specimen are digitized. Magnification is such that each field has approximately one and a half wavelengths of yarn segment visible. The image being analyzed is displayed to a video monitor, and points defining the edges of the yarns (roughly 12 per yarn) are identified by the operator using a mouse-and-cursor setup. An equation is smoothed through the points to approximate the yarn boundary. A polynomial was chosen for convenience, and was found to work well. The degree of the polynomial fit can be selected based on the waviness of the yarns; for the materials analyzed here, 7th degree polynomials were generally used. Figure 3 shows the functional fits to the yarn boundaries superposed on the original image; the white lines are the polynomial fits to the yarn boundaries.

Operator input was necessary to identify points on the yarn boundaries because there was little contrast between normal and transverse yarns in the images of the carbon-carbon composites studied here, and because complications are encountered in distinguishing between yarns that touch each other. Although operator input tends to slow the measurement rate, by making the input simple the time investment and accuracy proved to be efficient compared to the alternative computational investment. Examples of the operator time required are given below. An important goal was to minimize the sensitivity of the measurements to the operator. In this case the strategy of smoothing a function through the operator-selected points made the location of a particular point uncritical. Excellent fits to yarn boundaries were obtained; Figure 3 is entirely typical.

4.3 Extracting Information About Yarn Shape and Nesting

The second stage of the process takes the yarn boundary fits and extracts information. This part of the process is readily amenable to almost complete computer automation. Definition of yarn boundaries as described above results in an output file containing the polynomial coefficients for each yarn boundary segment. This information can be used by a number of separate programs to collect the desired distributions of yarn shape measures.

Both the top and bottom boundaries of the yarns are recorded since yarn thickness is not always uniform. As it seems desirable to have data reflecting the path of the yarn centerline, for

Yarn Shape Parameters

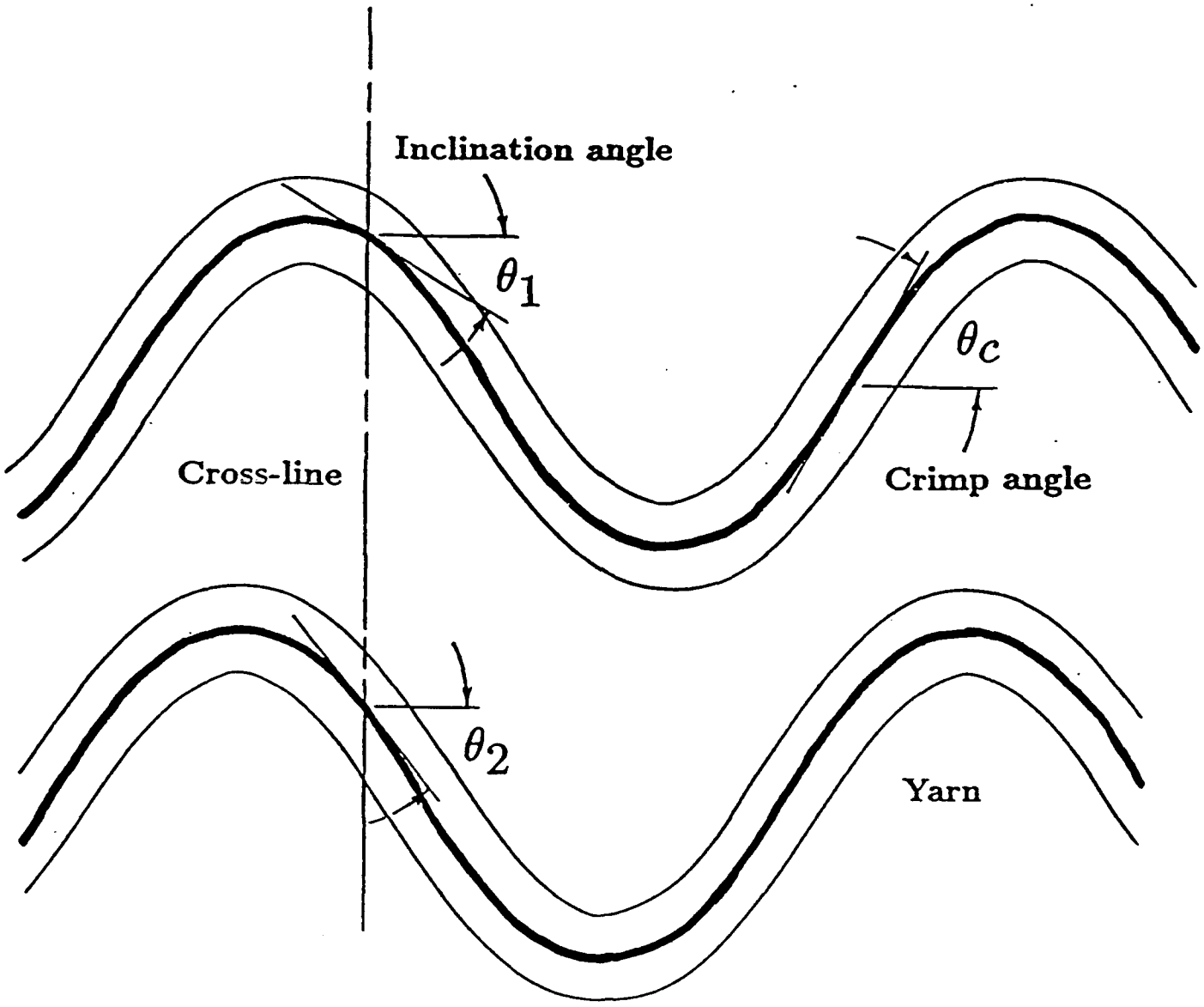

$\theta_1 - \theta_2 =$ Angle match

Figure 2: Definition of three measures of yarn shape.

each yarn segment the midpoint along the y-axis (defined as perpendicular to the plane of the weave) between the upper and lower boundaries is determined at 15 uniformly spaced intervals along the yarn. Another 7th order polynomial is fit to these midpoints and becomes the functional representation of the estimated yarn centerline.

Inclination angles are easily found from the first derivative of the polynomial fit. Sampling of the inclination angles along a yarn are taken at the intersections of "crosslines" and yarns. Crosslines are lines parallel to the y-axis, and traverse the complete image field. Placement of crosslines within 50 pixels of the edge of the image was avoided; inaccuracy near the edges results from misbehavior of the polynomial fit which has no constraints beyond the image boundaries. Further discussion of measurement accuracy is given below. The number of inclination angle measurements depends on the number of digital images analyzed and the number of crosslines chosen; the data presented below was collected from 25 crosslines randomly spaced per field.

The specimen initially is aligned by eye in the microscope stage. Because the average yarn direction (defined as the zero-degree, or x-axis, direction) is not accuratcly known *a priori*, the inclination angle data is shifted until the average is zero. This is not a completely satisfactory solution, however, since it assumes yarn shapes have symmetric inclination angle distributions. If this is not the case, the shifting to a mean of zero will give a false representation of the angle magnitudes, although the distribution shape will not be affected. Consideration of a saw-tooth waveform will make this clear. For the data presented below, it appears that the assumption of symmetry is reasonable; shifts were always less than 1.6 degrees.

Crimp angles are found by searching each yarn-shape function for inflection points. Points (digitized in pixel-unit spatial resolution) along each yarn centerline are polled for the first and second derivative at each point. Peaks or troughs are identified by the first derivative changing sign. Between a peak and a trough the inclination angle is measured wherever there is an inflection point revealed by the second derivative changing sign. Consistent with the definition of crimp angle, the largest inclination angle in each peak-to-trough interval is recorded as the crimp angle. To compensate for initial specimen misalignment, crimp angle distributions are shifted by the same shift required to bring the inclination angle distribution to a mean of zero degrees.

Angle-match distribution is calculated using a slight variation of the crossline method. Along a single crossline, inclination angle is recorded along with the angle difference between adjacent yarns. The data consists of two columns, the first containing the inclination angle of the first yarn, and the second containing the inclination angle difference between this first yarn and its lower neighboring yarn.

All of these angle measurements have proven to be accurate and reproducible. Based on test cases involving known angles, the uncertainty of the angle measurements is estimated to be within +/- 1 degree. From a series of repeated measurements, in which the operator starts from the same image but re-defines the yarn boundaries each time, reproducibility of the angle measurements is estimated to be about +/- 0.5 degrees (if the edges of the image are discarded). Similar reproducibility is found between experienced operators.

4.4 Other Measures

Other morphological measures are available from the functional fits to the yarn shape. Of particular interest to modeling efforts is approximating the yarn shape with a sinusoid. In the examples described below, a sinusoid was fit to the yarn-shape data using a least-squares method; specifically,

Figure 3: Illustration of the functional fits to the yarn boundaries. The white line are the fits superposed on the original image.

a modified Levenberg-Marquardt algorithm, available from the SLATEC numerical methods library [17], was incorporated into a simple code to fit yarn segment shapes to the function,

$$y = A\sin(\frac{2\pi x}{l} + \phi)$$

where the amplitude (A), wavelength (l), and phase angle (ϕ) are the adjustable parameters.

Yarn volume fraction measurements are readily available from the first stage data using established methods [18]. Information about yarn wavelength and amplitude distribution can also be extracted from the yarn shape functions. These measures are not illustrated here.

The two-stage approach—fitting functions to the yarn boundaries, and then extracting information from the functions—has proved to be efficient; it allows the stored yarn-boundary fits to be used several times to extract a variety of information.

5 Examples

The techniques described are applied to a carbon-carbon composite to provide illustrative inclination-angle, crimp-angle, and angle-match distributions. The material is a laminate of plain-weave carbon-fiber cloth in a carbon matrix. The cloth comprises mutually orthogonal warp and fill yarns in a plain (2-harness) weave pattern with 28 warp yarns and 22 fill yarns per inch. The warp directions of each cloth layer are parallel. The composite is the same as that studied by Jortner [14], who showed that yarn shapes can vary significantly from panel to panel. Each sample studied here came from a different panel.

For each illustrative measurement distribution, fifteen digital images were analyzed. Sample are sectioned normal to the plane of the laminate and par l to either the warp or fill direction. Standard metallographic polishing techniques were used to p.epare specimens for microscopy. Each image field represented a 2.25 x 1.68 mm section of the specimen, resulting in a representative sample area of 57 mm^2. Creating the polynomial fits to the yarn boundaries requires 5 to 8 minutes per image analyzed. Analysis for inclination angle, crimp angle, and angle-match takes less than a minute each per field. Each specimen provided two sets of measurements—one for the warp yarns and one for the fill yarns. Sample size (number of angle measurements) for an inclination-angle distribution was approximately 1500. Sample size for a crimp-angle distribution was about 120. Total analysis time for each specimen orientation was, on the average, two and a half hours.

5.1 Inclination-Angle and Crimp-Angle Distributions

Figures 4 and 5 show the inclination-angle distributions for fill and warp yarns of panel A. The fill-yarn inclination-angle distribution shows two peaks, at -28 and 32 degrees, with a low at zero and a standard deviation of about 22 degrees. The shape of the distribution is expected; it is similar to the distribution predicted if the yarn shapes were sinusoidal. For sine waves with identical amplitudes and periods, peaks in the inclination angle distributions occur at the crimp angles. If the amplitude-to-wavelength ratios were normally distributed, the inclination angle histogram would be very similar to Figure 4, indicating that fill-yarn shape for this material can be represented well by a sine wave. The fill crimp-angle data for sample A, shown in Figure 6, show a fairly sharp peak near 30 degrees. Note that crimp angles are plotted as absolute values since this is all that current use of the data requires.

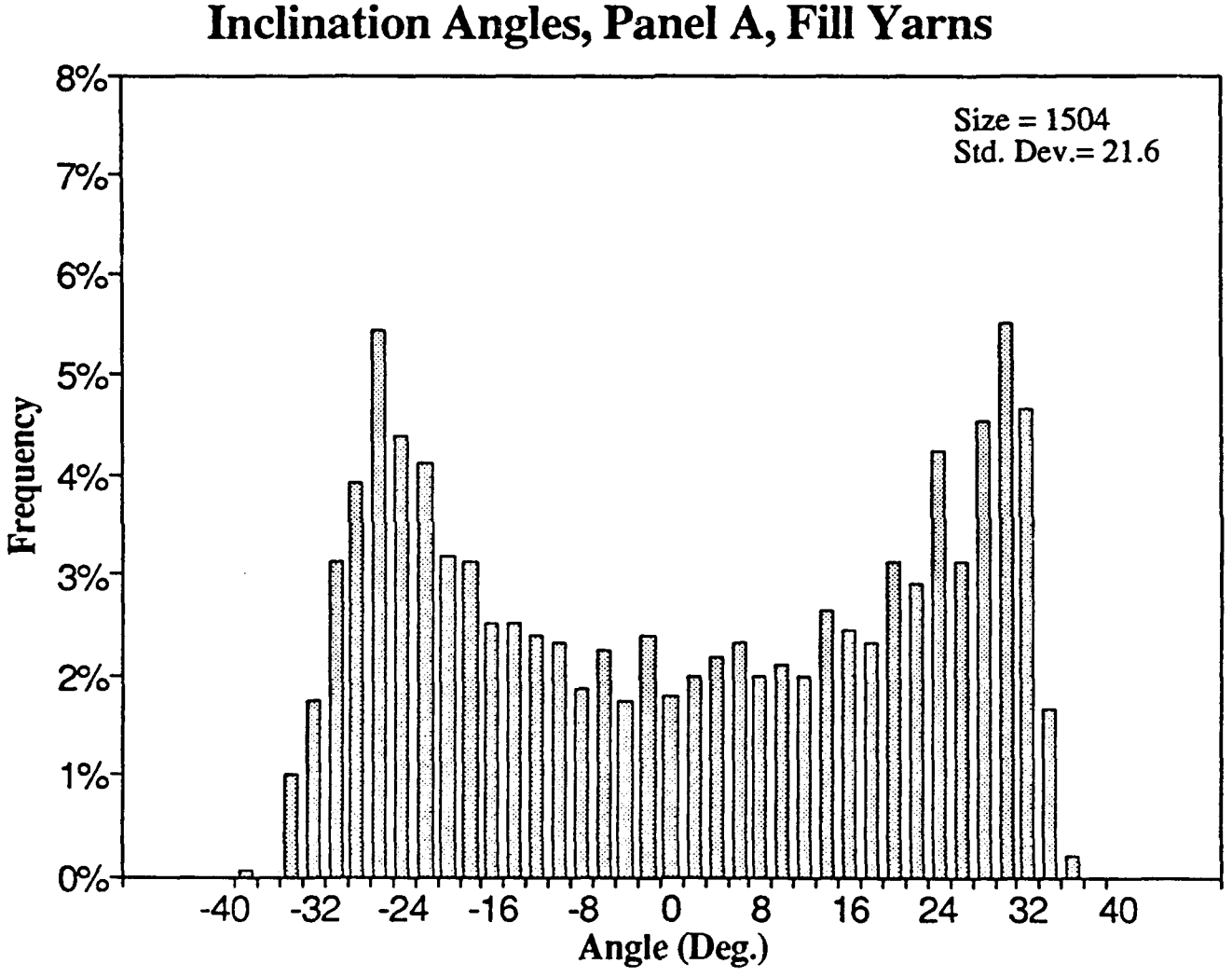

Figure 4: Fill yarn inclination angle distribution from Panel A. The shape of the distribution is similar to the distribution predicted for sinsoidally shaped yarns.

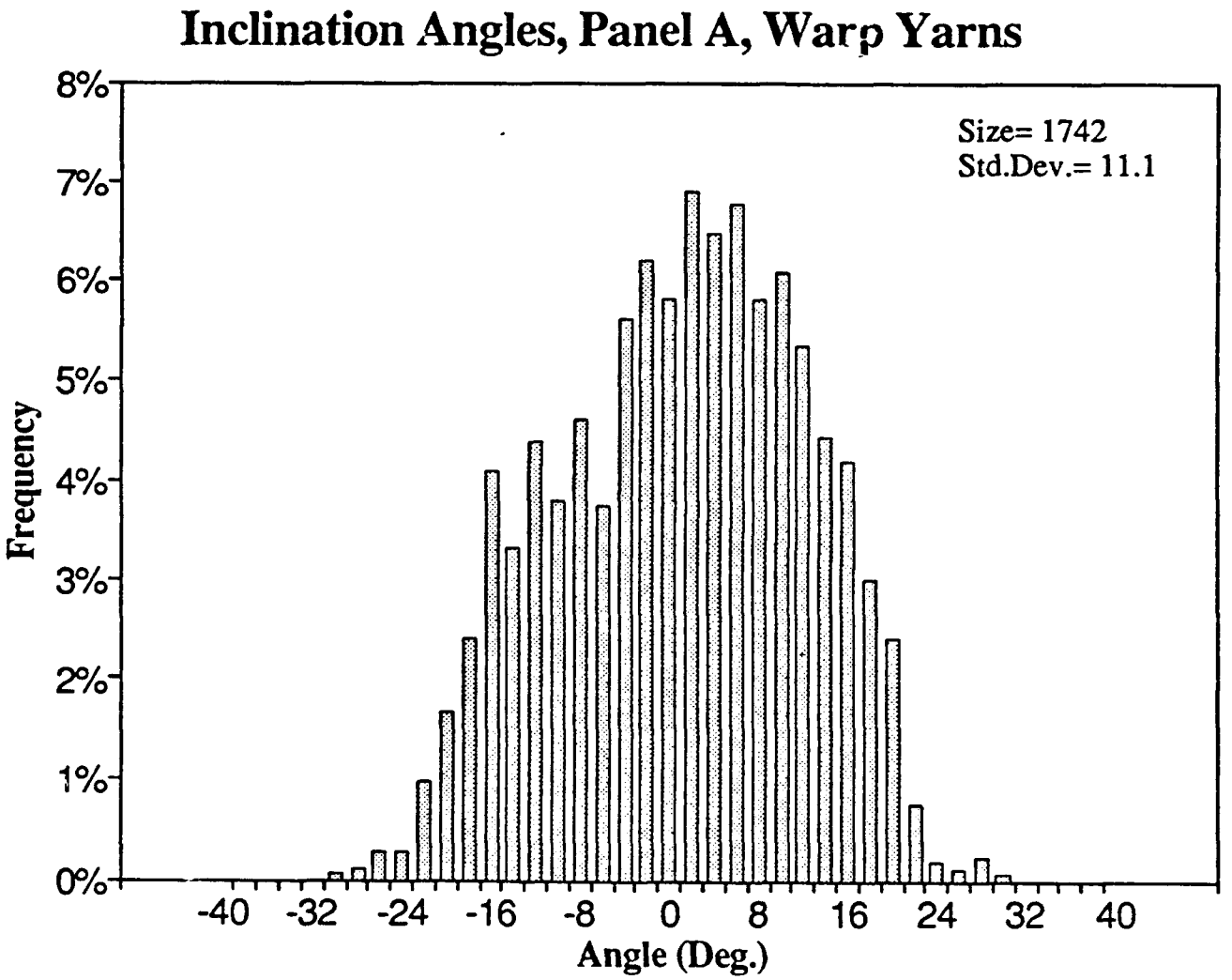

Figure 5: Warp yarn inclination angle distribution from Panel A. Compared to the fill yarns (Figure 4), the warp yarn shape is substantially different: flatter and less "sinusoidal".

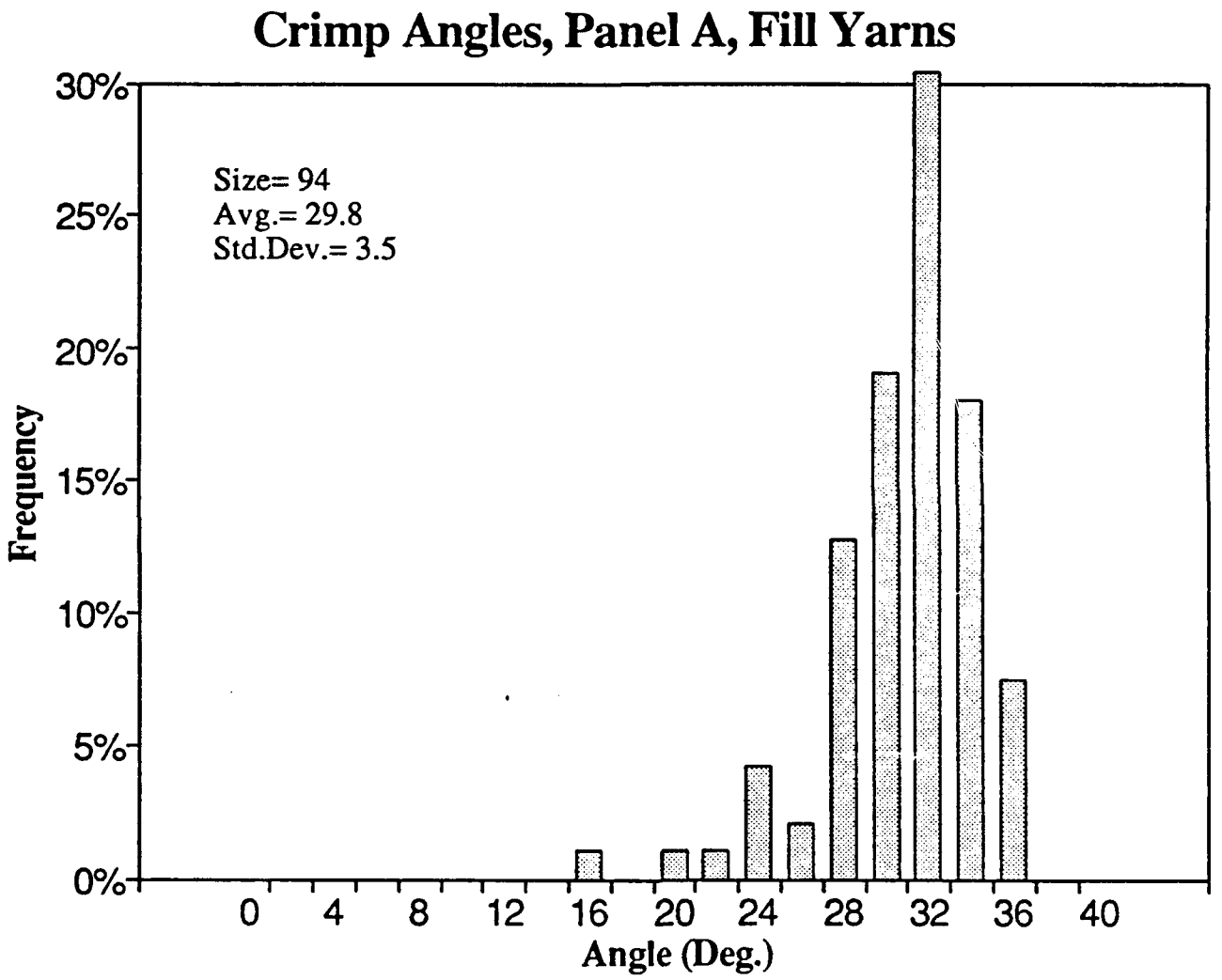

Figure 6: Crimp angle distribution from the fill yarns of Panel A.

In contrast, the warp-yarn inclination-angle distribution for panel A has one major peak centered about zero degrees, and a standard deviation of only about 12 degrees. The relative narrowness of the warp distribution indicates that the warp yarns in material A are much straighter than the fills; the single peak shows that the warp-yarn shape cannot be accurately represented by a sine wave. The warp crimp angles (Figure 7) are significantly lower and more widely scattered than the fill crimp angles.

Differences between fill and warp distributions derive from the unbalanced spacing of the weave and from effects of nesting during laminate compaction. Measurements from mounted and polished samples of resin-prepregged cloth, of the type used to make this carbon-carbon laminate, show the warp inclination-angle distribution to have been closer initially to sinusoidal—note the two peaks in Figure 8. The results quantitatively confirm the observation [16] that, in this material, warp-yarn shapes usually are distorted more than are fill-yarn shapes.

The variability of such laminates is illustrated by measurements on a sample from panel C, ostensibly the same material as panel A. Figures 9 and 10 show inclination-angle distributions that hardly distinguish between warps and fills; the warp inclination-angle data also shows the sinusoid-like double peak. Some small differences show up in the respective crimp-angle data for panel C (Figures 11 and 12); the average crimp angle is slightly lower, and the distribution noticeably wider, for the warps.

Another variation is illustrated by the distinctly unsymmetric inclination-angle distribution, Figure 13, for the warp yarns in yet another panel (Panel B) of the same type of laminate. The warp yarn shapes in this specimen are skewed, perhaps by shear during compaction of the laminate.

5.2 Angle-Match Distributions

Figure 14 is a perspective sketch, based on microscopic observations, of a typical section of a plain-weave laminate. It illustrates that the nested yarn shapes can be quite complex. To gain some insight into the three-dimensional shape of such yarns, yarn cross-sections were outlined on magnified views of a series of carefully spaced sections through a sample, and the 3D yarn shape reconstructed with the aid of computer-aided-drawing software. The example in Figure 15 shows fairly consistent cross-sections. There are some noticeable changes in yarn width (when viewed from the top), but as the yarn is thin at the edges, these width variations do not involve much material. The construction of such 3D representations is quite time consuming and does not, in the current implementation, provide much usable quantitative data. It does, however, serve to remind that the wave-path parameters studied here are a limited characterization of actual yarn shapes.

Angle-match data are intended to characterize the nesting of adjacent cloth layers, two by two. In addition to measuring the angle difference between neighboring yarns, the absolute angle of the yarns must also be recorded. For instance, an angle-match of zero degrees could be recorded for neighboring yarns segments both at 10 degrees as well as for two yarn segments both at 45 degrees, but the effect on composite properties for both cases may be different. The solution to this problem is to plot the distribution of angle-match with respect to the inclination angle of the first yarn. The result is a histogram on two variables, presented as a contour plot like the ones shown in Figures 16 and 17 for the fill and warp yarns of panel D. Here, θ represents the angle of the first yarn and $\Delta\theta$ the absolute value of the angle-match between this yarn and its lower neighbor.

Such plots are quite complex; they incorporate an absolute-value version of the inclination-angle distribution plus the angle-match data. For yarns that are approximately sinusoidal, like the fill

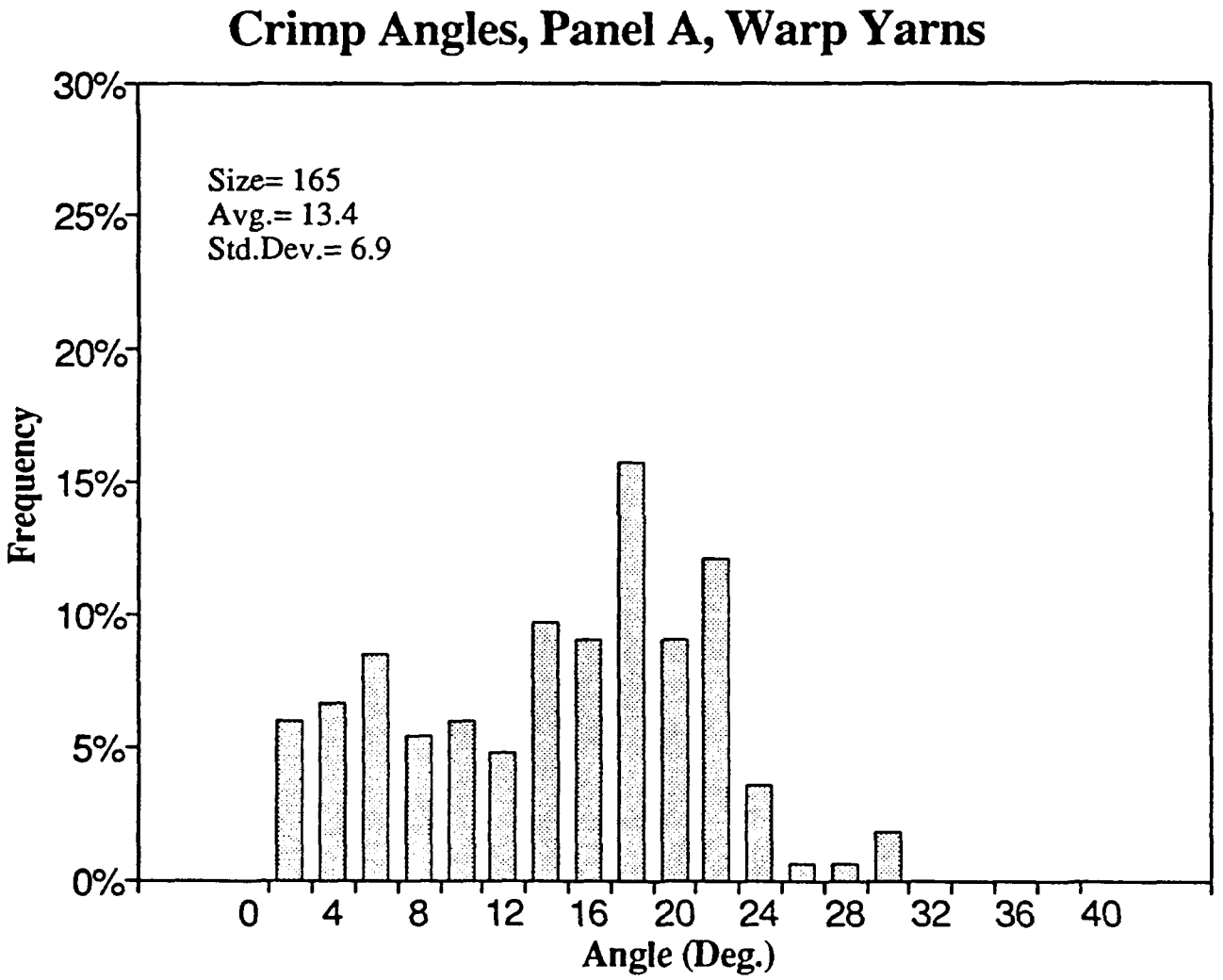

Figure 7: Crimp angle distribution from the warp yarns of Panel A. Compared to the fill yarns, the warp crimps are considerably smaller and more scattered.

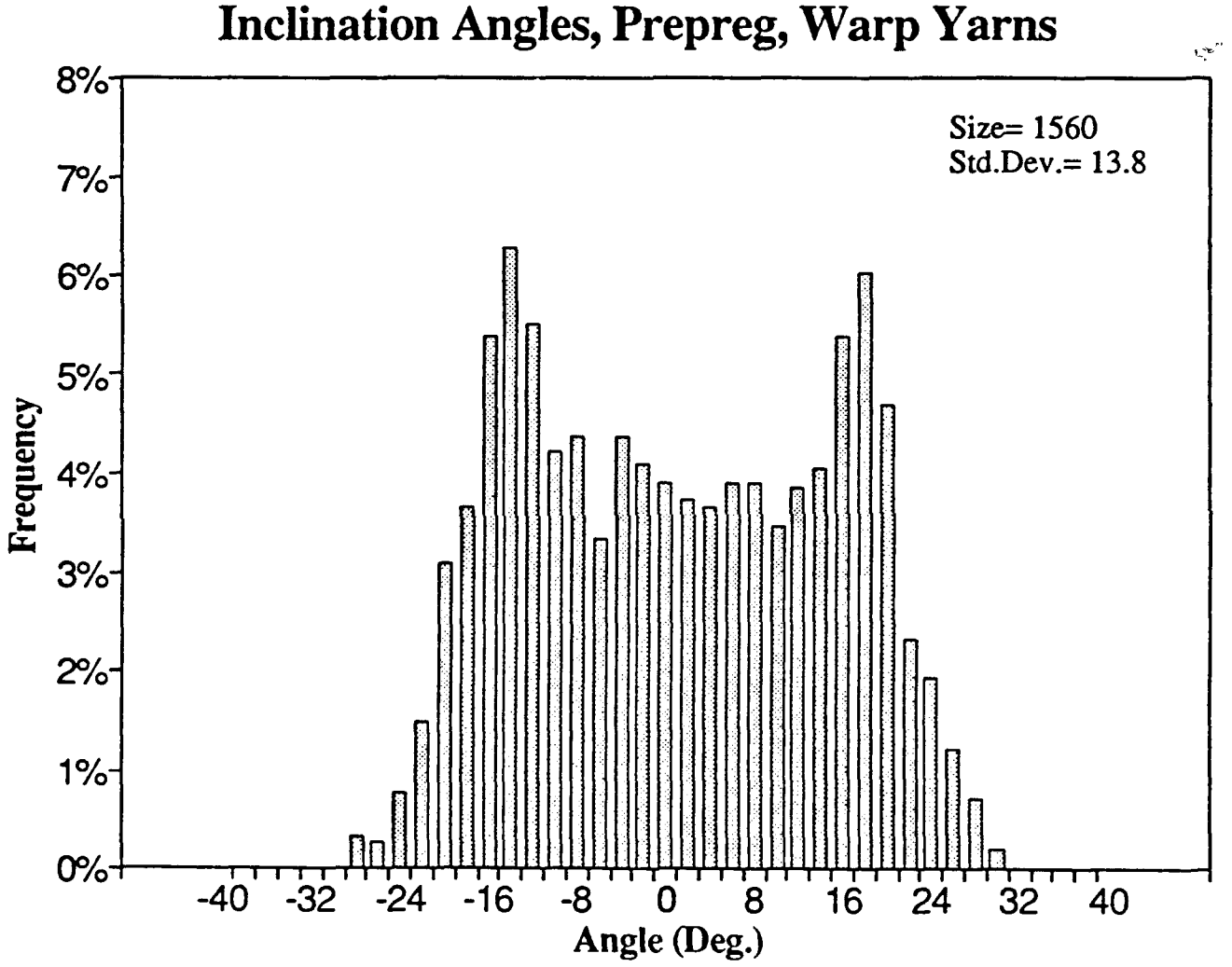

Figure 8: Inclination angle distribution of warp yarns in the resin-prepregged cloth, prior to lamination, used to produce Panel A laminate. The distribution shows a yarn shape closer to sinusoidal, and illustrates how yarn shape can change during processing.

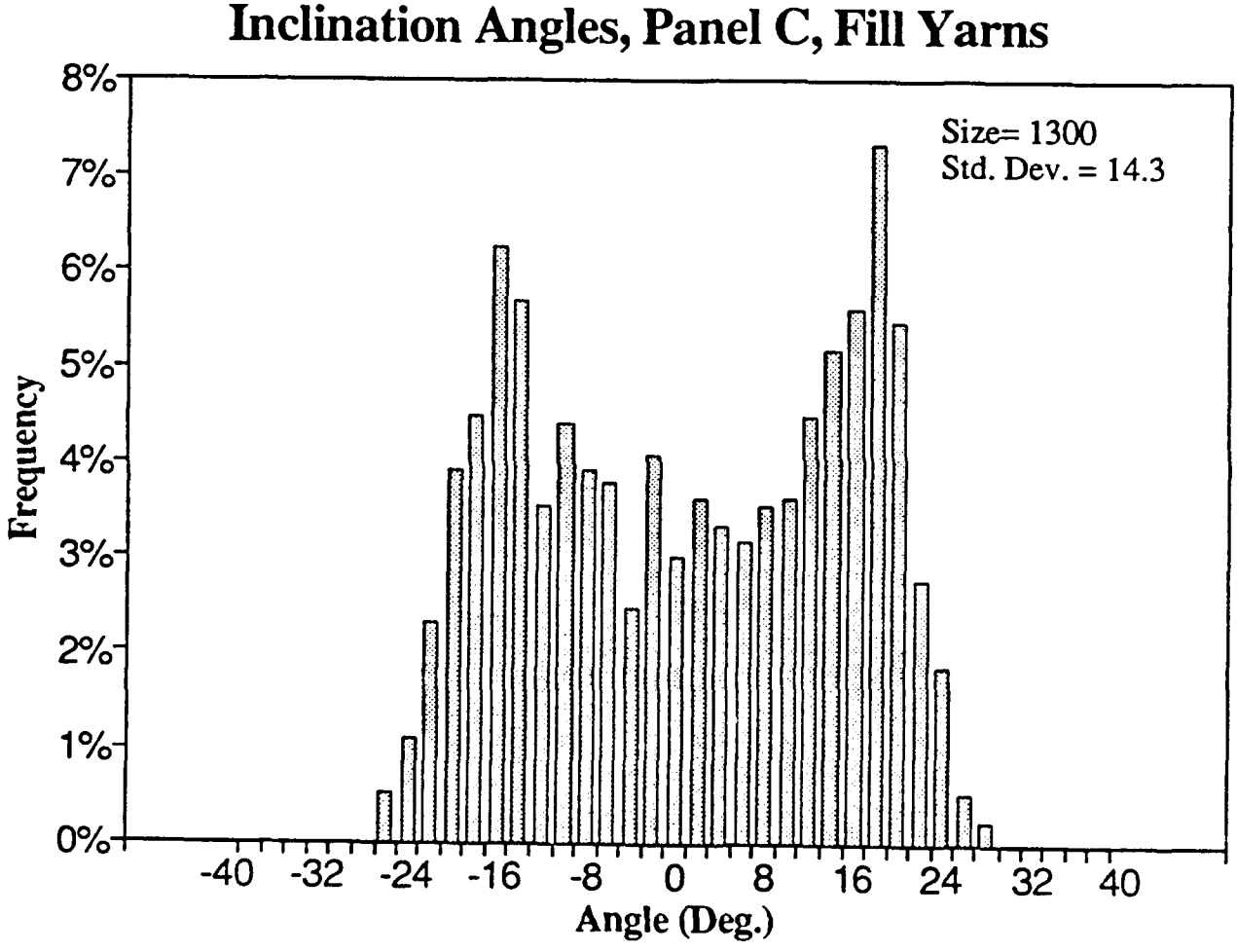

Figure 9: Fill yarn inclination angle distribution from Panel C. This material is ostensiblly the same material as panel A, but comparison of the inclination angle distributions shows that there are substantial differences in yarn shape.

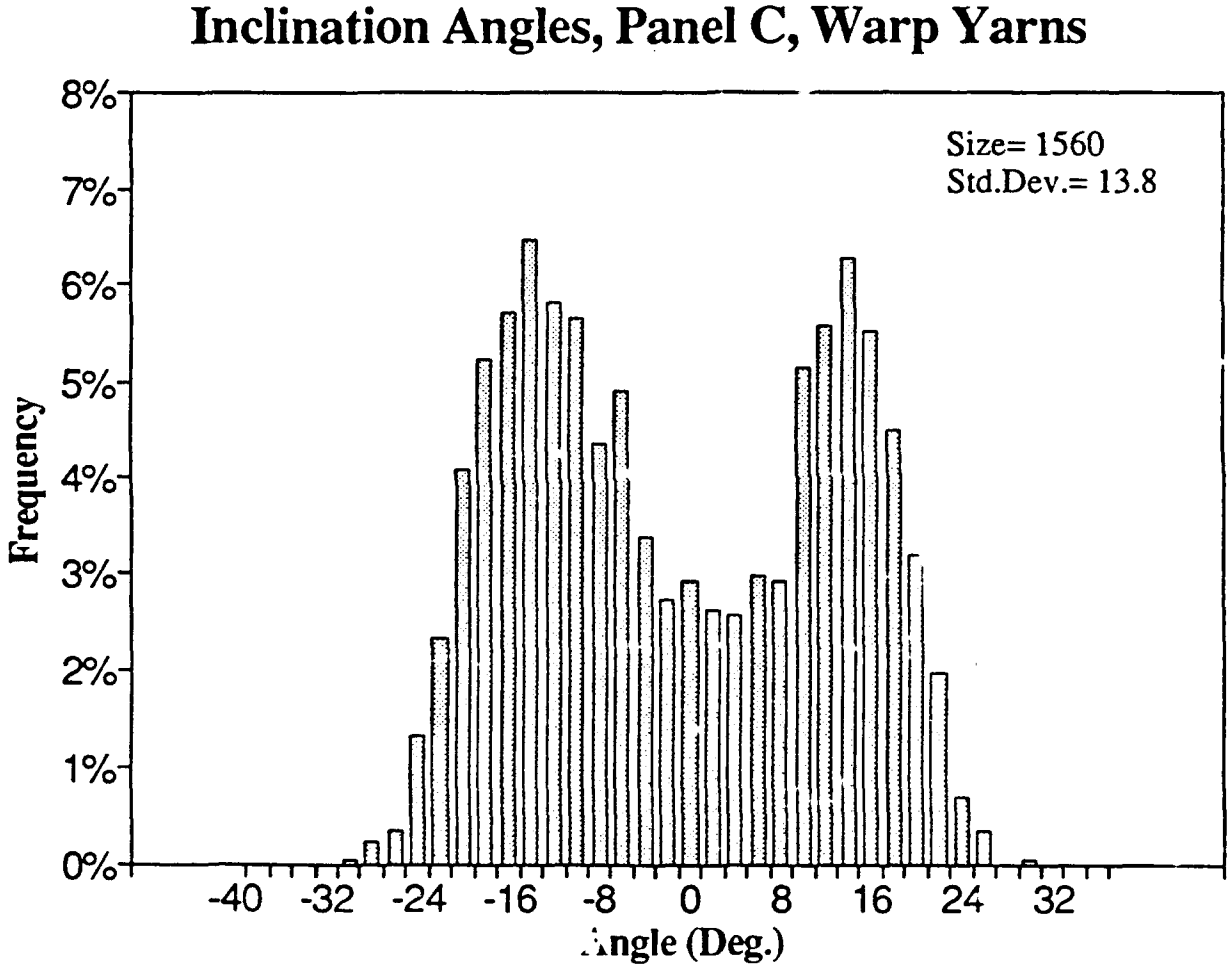

Figure 10: Warp yarn inclination angle distribution from Panel C. In this panel the warp and fill yarns appear to have about the same shape. Contrast this to Panel A.

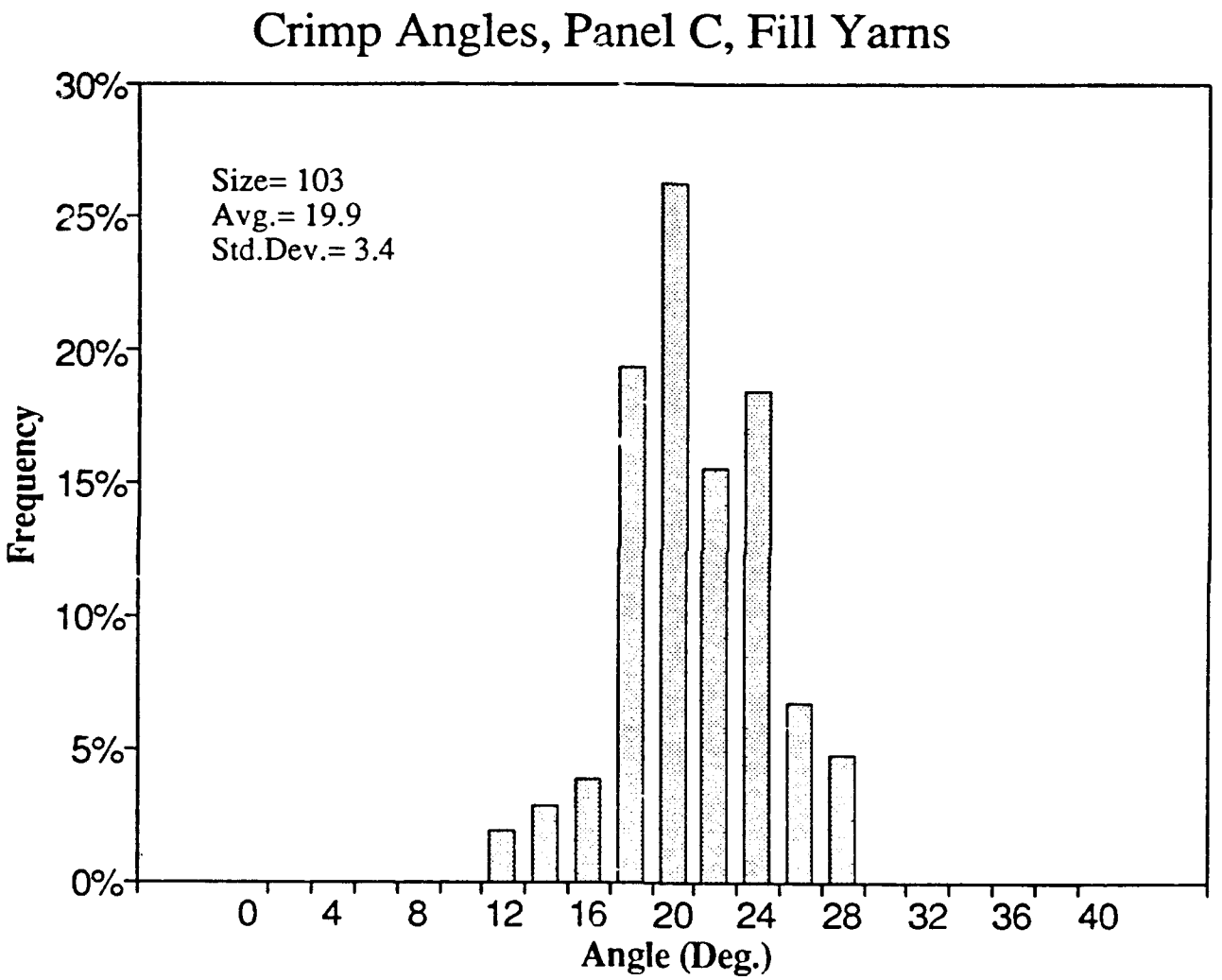

Figure 11: Fill yarn crimp angle distribution from Panel C.

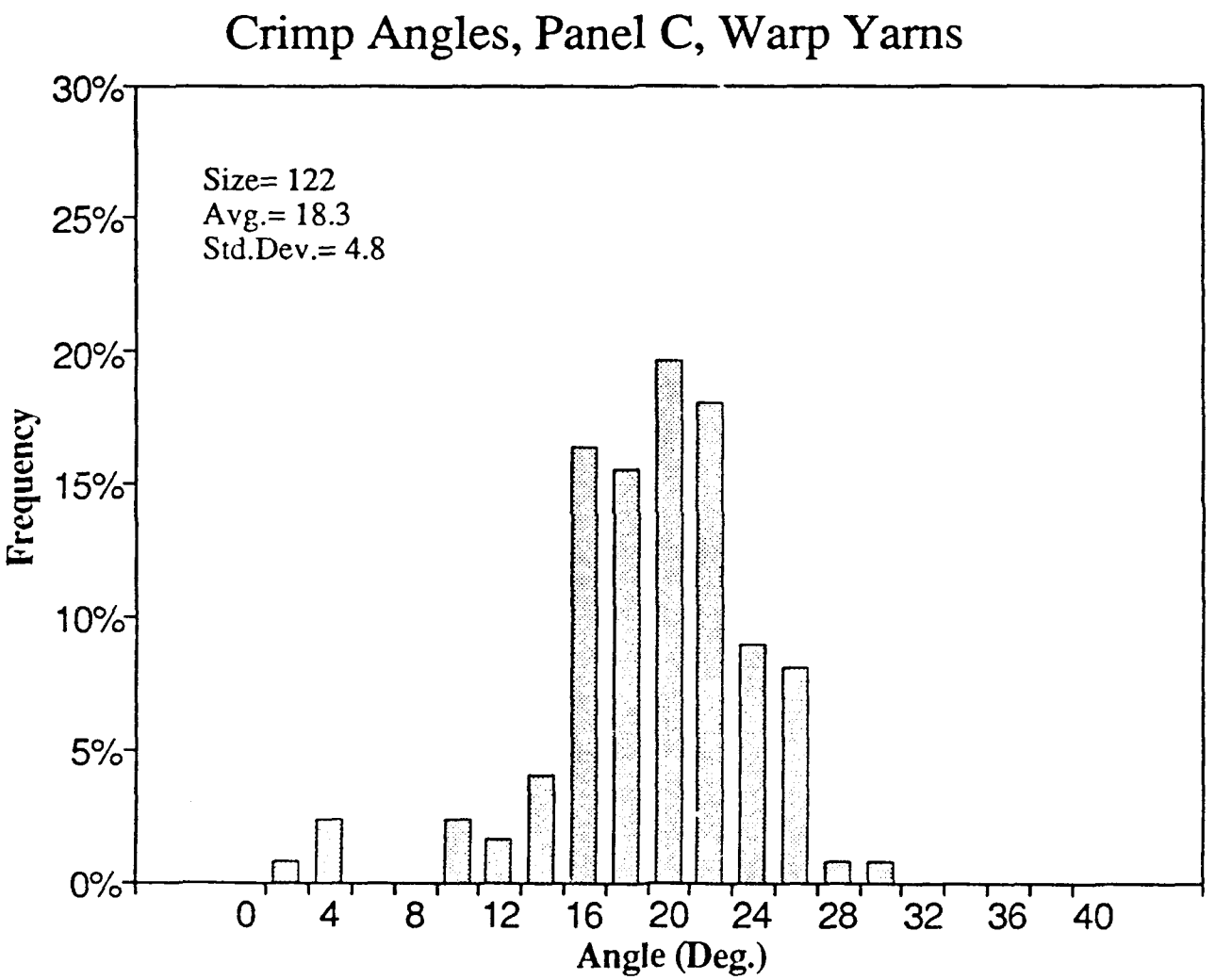

Figure 12: Warp yarn crimp angle distribution from Panel C. In this case the warp and fill crimps are similar, with the warps being somewhat flatter and more scattered.

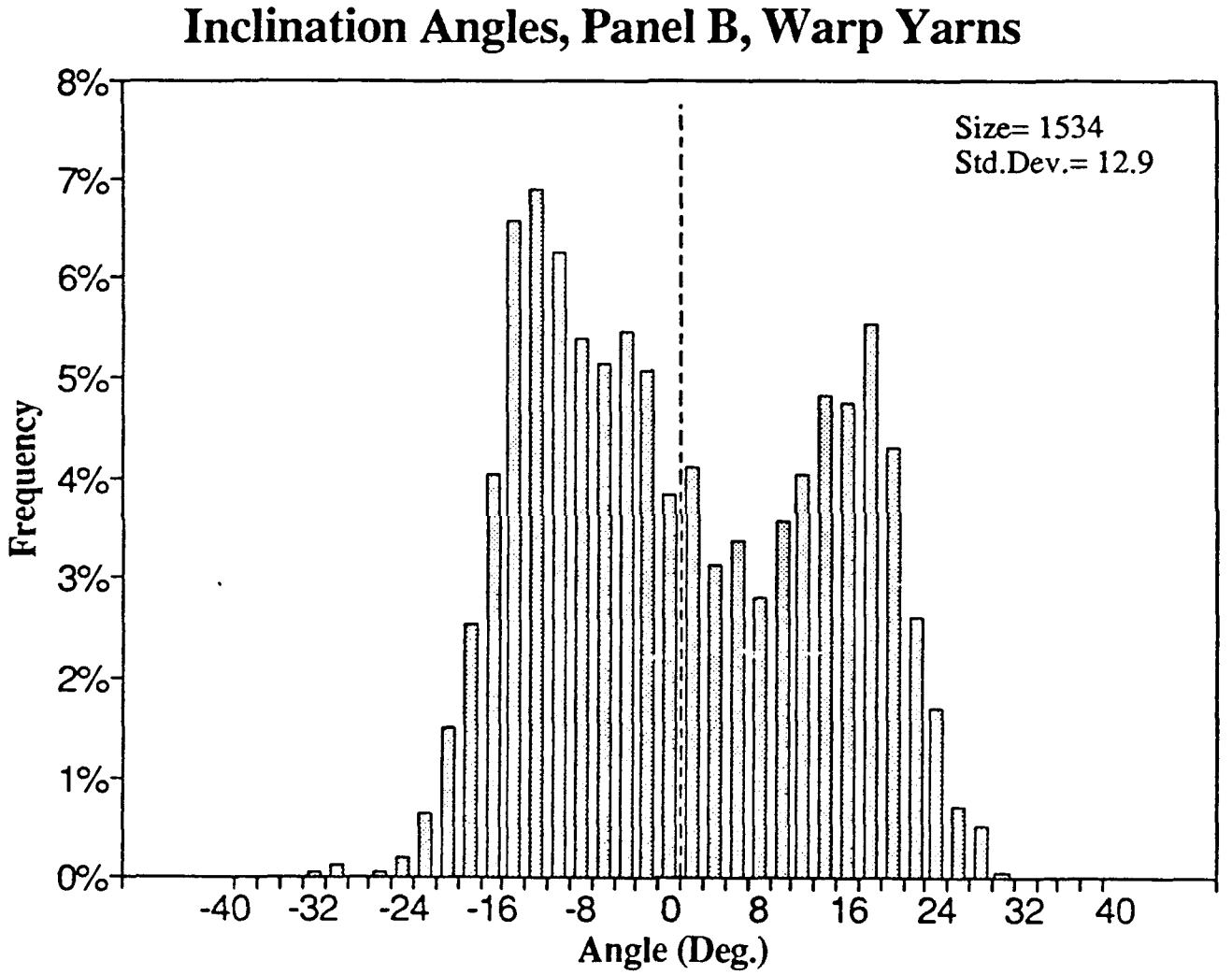

Figure 13: Inclination angle distribution of the warp yarns in Panel B. Note how the distribution is skewed, indicative of a somewhat sawtoothed yarn shape. This skew may have been caused by shear during processing.

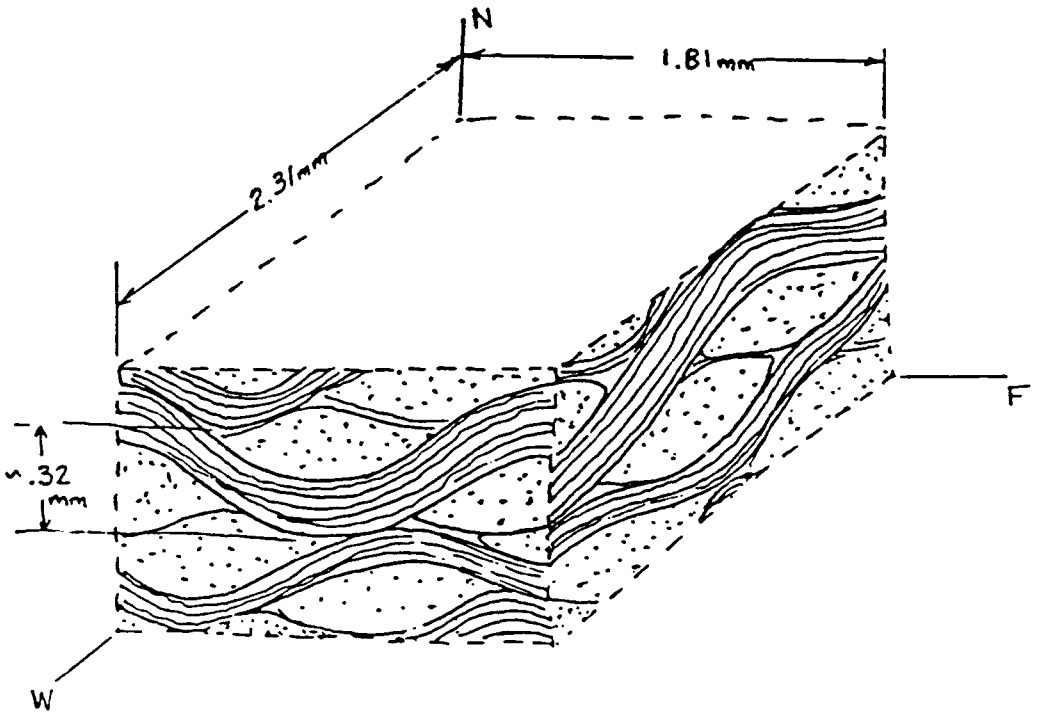

Figure 14: Sketch of a typical section of a plain-weave reinforced composite (Taken from [16])

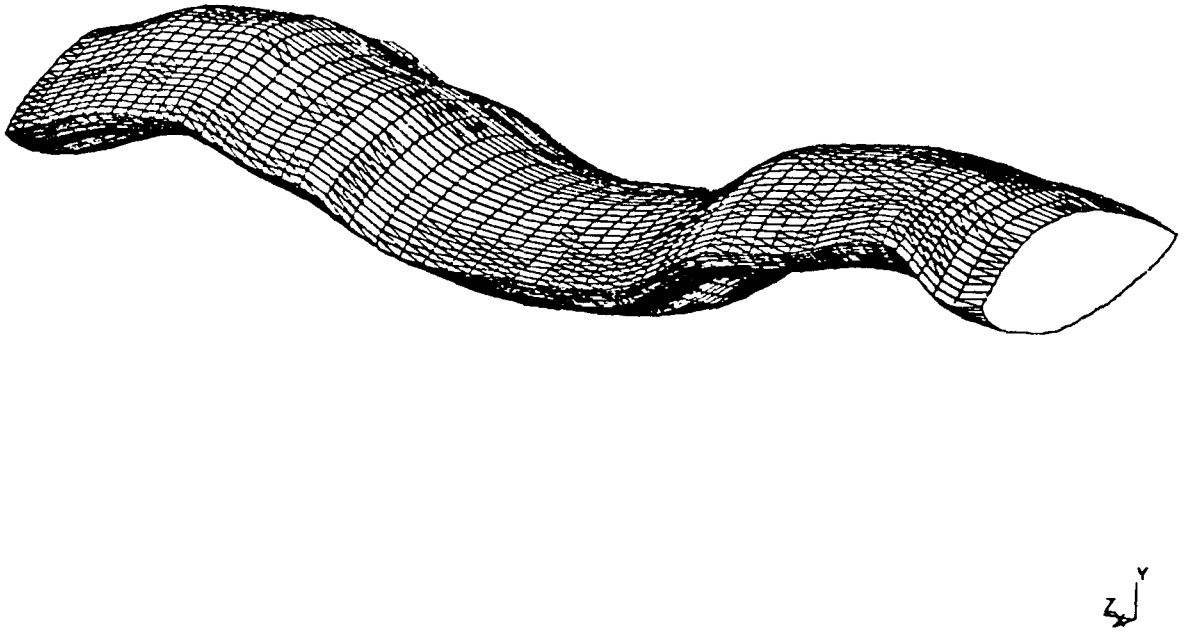

Figure 15: Three-dimensional reconstruction of a yarn which is part of a plain-weave reinforced carbon-carbon composite. Reconstructed from 12 serial sections taken along the yarn axis.

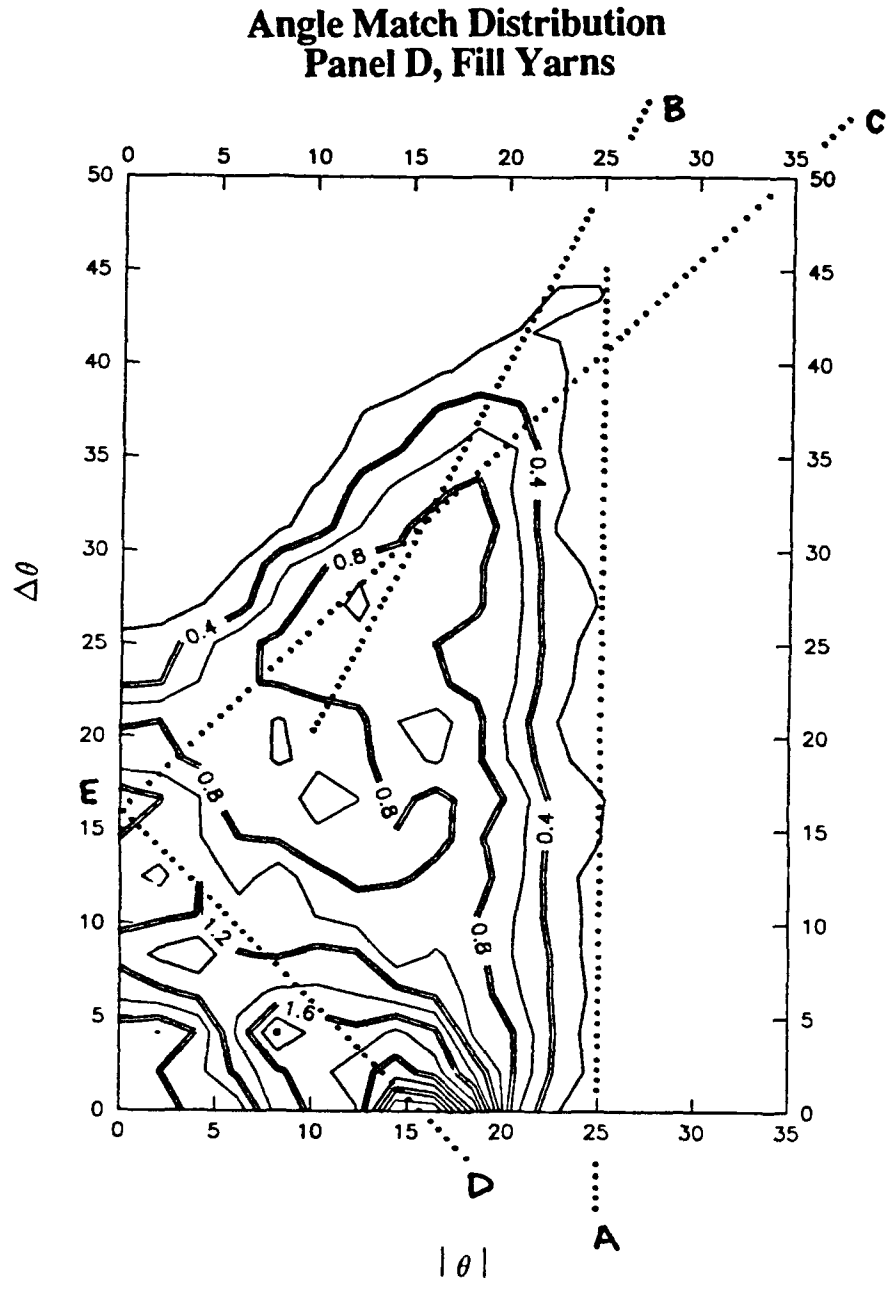

Figure 16: Angle-match distribution from Panel D fill yarns. This data is a measure of yarn nesting. Interpretation of the plot is given in the text.

yarns of Panel C, the contour plots would indicate the degree of phase-match in the alignment of neighboring yarns. A higher distribution along the zero delta theta line would indicate a high degree of in-phaseness while a high distribution at a large $\Delta\theta$ would indicate out-of-phaseness. The lines drawn in Figure 16 illustrate other features revealed in the contours. Line A is a boundary showing the maximum inclination angle. Points that fall along line B represent neighboring yarns that are completely out-of-phase. If the shape of a yarn is completely unaffected (i.e. not nested) by its neighbor, then the maximum frequency should fall along line CDE; for any inclination angle θ, the most likely inclination angle of the neighbor yarn is the peak frequency of the inclination angle distribution.

As an example of interpretation, the high distributions along $\Delta\theta$=0 of Figure 17 indicate a high degree of contact between yarns. The peak near $\Delta\theta$=0, θ=10 degrees suggests that the yarns were touching at this angle. Visual examination qualitatively confirms this result.

For materials with irregular yarn shapes, angle-match distribution may be considered an independent composite characteristic, not necessarily related to phase match (which may have no meaning in such materials).

More work is needed in interpreting angle-match data; part of this effort will require measurements from more materials to provide a better context for interpretation. Other measures of nesting may be imagined, and it is not clear which is best. For example, the angle-match contours could be collapsed to the θ= 0 line, making interpretation easier, but giving up information about the magnitudes of the yarn orientation angles. It may be noted that such a distribution in principle contains the same information as an angle-match distribution gathered along a single "infinite" length crossline. While angle-match contours are difficult at present to interpret, they provide such a wealth of information about yarn orientation and ply nesting that it seems useful to pursue this technique for characterizing yarn morphology.

5.3 Waveform Descriptions

Sinusoidal approximations to yarn shape are illustrated in Figures 18 and 19. The first figure gives an example of the fits obtained for three yarn segments of panel C. The second figure shows the distribution of fitted wavelengths for all of the warp-yarn segments examined for panel C. Approximating the yarn shapes with sine waves gives distributions of wavelengths and wavelength-to-amplitude ratios. The mean values of each would represent the best sine-wave approximation for the sample's mean yarn shape, while the variances would indicate the uniformity of the yarn shape. To the extent that sinusoidal approximations of yarn shape often are assumed in modeling, the technique presented here provides a way of inputting actual yarn-shape measurements into models. However, as some of the inclination-angle data demonstrates, a sinusoidal approximation to yarn shape is not always justified.

Another way to define an "average" or "effective" yarn shape, without assuming a sinusoid, is to construct it directly from the inclination-angle distribution. Inclination angle distributions give the fraction of yarn length, as projected onto the x-axis, that has a given inclination angle. A single wave that has the same inclination-angle distribution can easily be constructed to give the same distribution. The simplest such shape is formed by linking angled elements, in appropriate proportions, so the y-position increases monotonically from zero-amplitude to the maximum, then monotonically decreases back to zero. Note, however, that many other shapes could be constructed to match the same inclination angle distribution. As an example of this approach, Figure 20 shows

Angle Match Distribution
Panel D, Warp Yarns

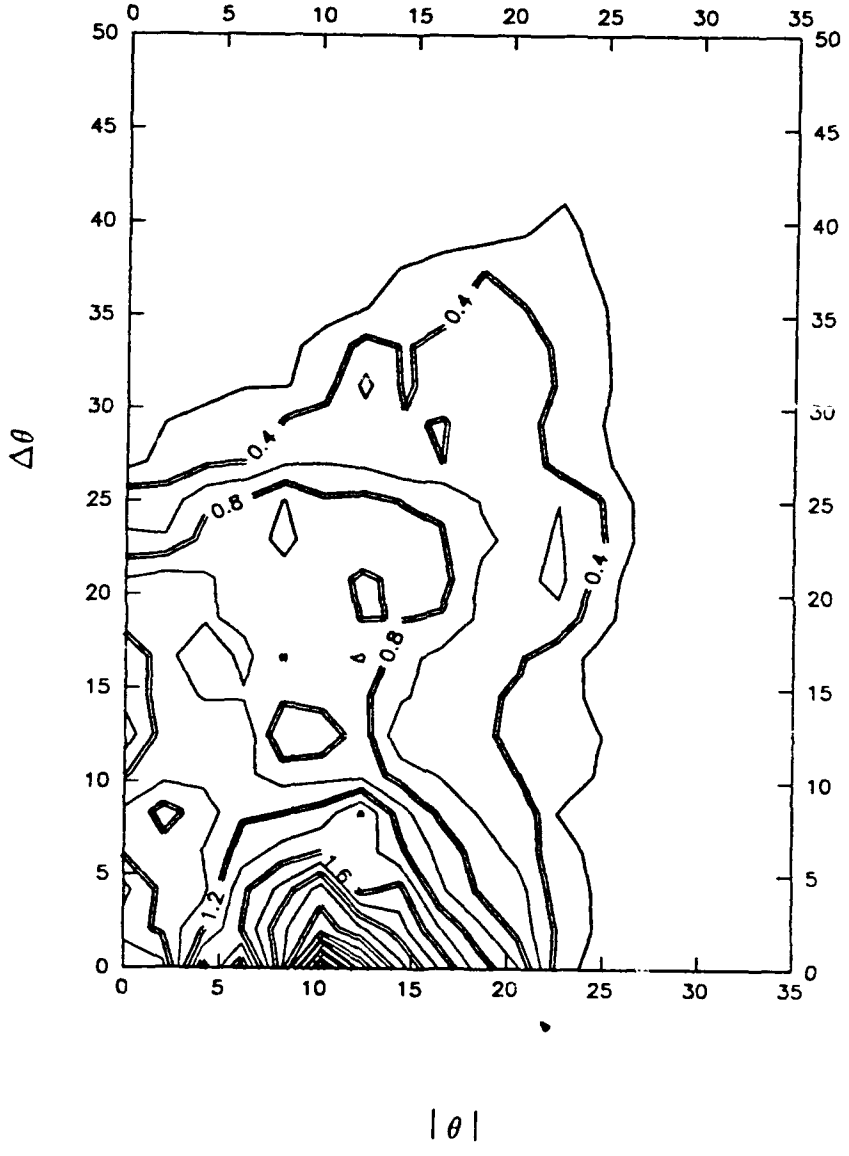

Figure 17: Angle-match distribution from Panel D warp yarns. The high concentration near $\Delta\theta=0$, $\theta=10$ degrees suggests that the yarns were touching at this angle.

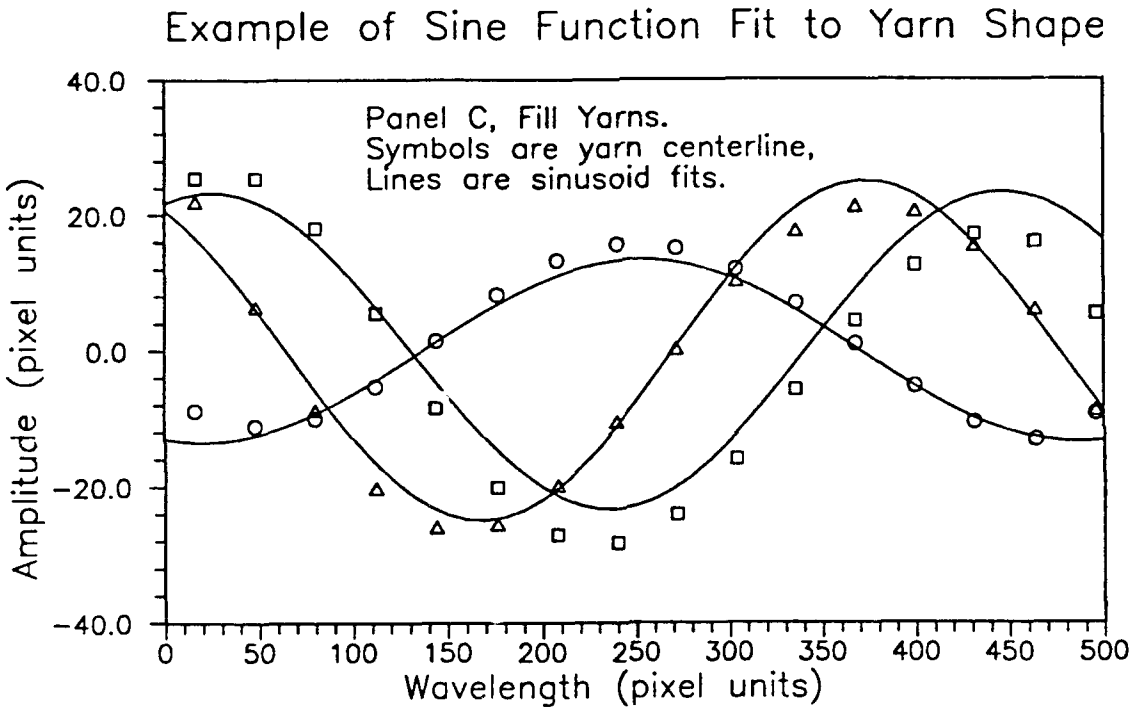

Figure 18: Example of the sinusoidal fit to warp yarn segments shapes of Panel C. Sinusoids fit to actual yarn shapes are provide a convenient representation for modeling, but still retain a connection to the actual morphology of the material.

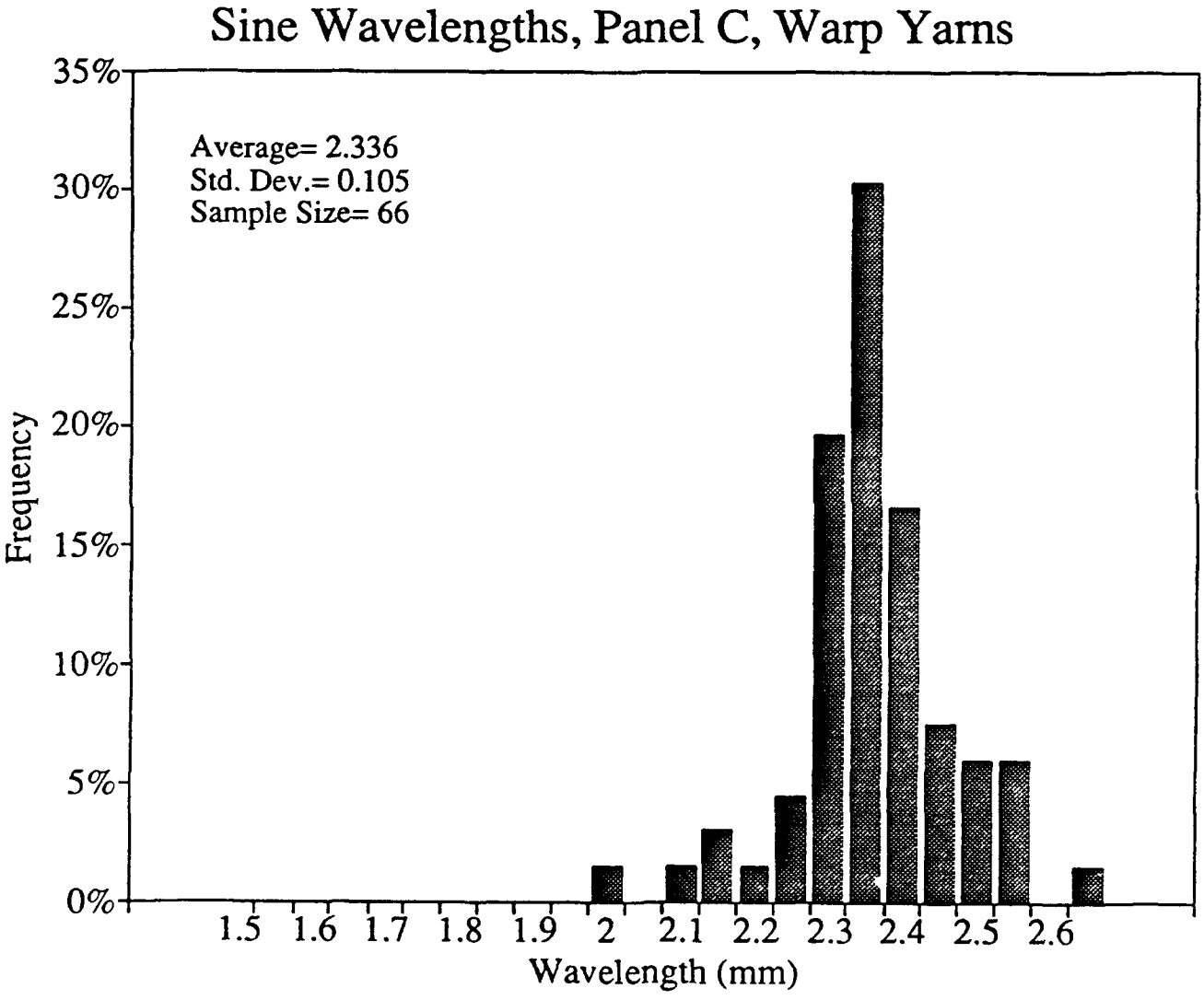

Figure 19: The distribution of sinusoidal wavelengths that have been fit to the yarns of Panel C. Data on the distribution of best-fit amplitudes is also available but not shown.

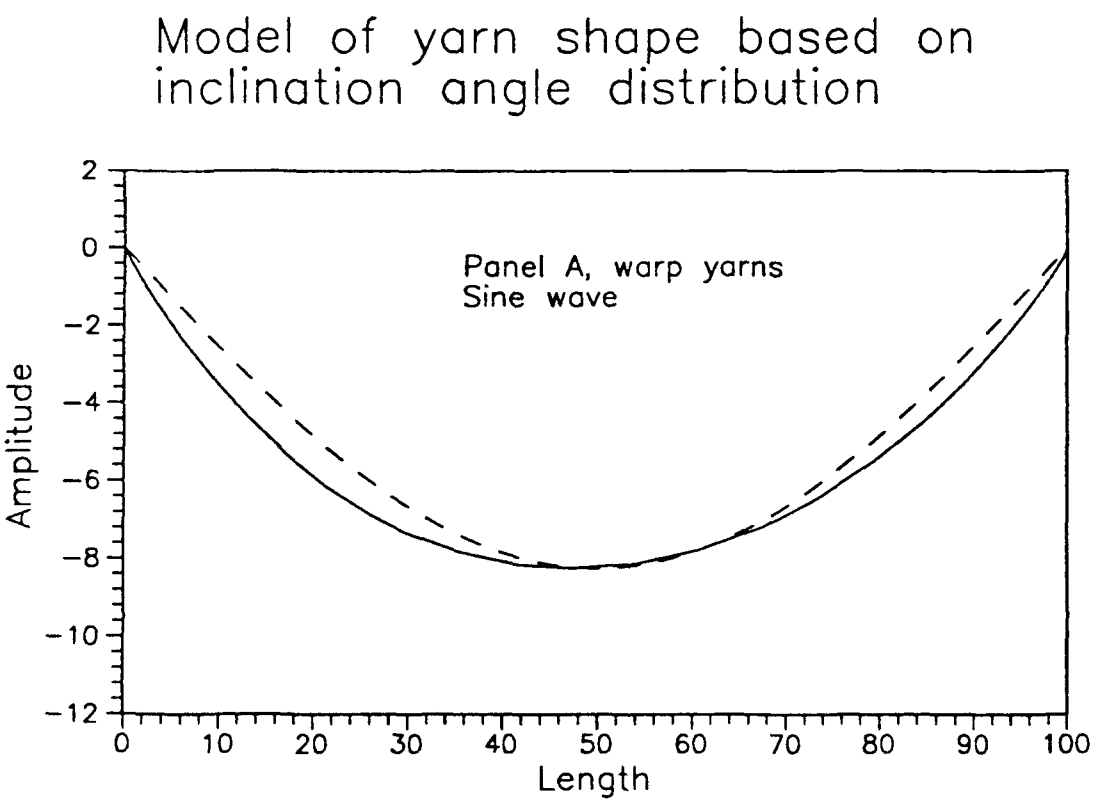

Figure 20: Creation of an "average" yarn shape based on the inclination angle distribution of Panel A warp yarns. The units are arbitrary. The dashed line shows a sine with the same amplitude and wavelength.

a shape that corresponds to the inclination-angle distribution for the warp yarns of Panel A; for comparison, a sinusoid having the same wavelength and amplitude also is shown.

The quest for a single effective yarn shape for each yarn direction (warp or fill) is motivated by the structure of existing models, which deal with a fully defined unit cell (or repeating volume element) of the material. The statistically distributed nature of the data shown here implies that less deterministic models may be preferable for analyzing cloth-reinforced laminates. While the forms that such stochastic models might take can only be imagined at present, some potential benefits can be sketched. For example, a mean yarn shape may prove adequate for predicting bulk constitutive responses at low stress levels; however, at higher stress levels, localized damage (presumably influenced by local inclination angles and nesting) would influence strain responses in ways not predictable from an effective yarn shape. Similarly, fracture in some modes may be a function of extreme values of inclination angle. Thus, the variance of yarn shape would enter into predictions of damage-related stress-strain nonlinearities and fracture. Even with regard to constitutive relations at low-stress, quantification of nesting and its variance may prove necessary to select the type of model (eg, stiffness- or compliance- averaging, or some alternate) and to define the unit-cell geometry that would best predict bulk elastic constants.

6 Conclusions

Because yarn shape and nesting is likely to have a strong influence on woven-reinforced composite properties, it is desirable to have a method for quantifying yarn morphology and an efficient way to make the measurements. Three measures of yarn morphology were developed here—inclination-angle distribution, crimp-angle distribution, and angle-match distribution. Several other measures of yarn shape were discussed, including best-fit sinusoidal descriptors, and no doubt others could be invented. Additional effort, involving both morphological description and modeling, would be necessary to settle on the most relevant set of measures.

Computer-aided image-analysis techniques have been developed to measure yarn shape. The application of digital image processing provides the ability to quickly, accurately, and routinely make these measurements at statistically significant sample sizes. While the present method does require operator input, the time required is not large and the sensitivity of the measurements to operator accuracy is not acute. The proposed method, which involves the fitting of functions to the wave paths of yarns, facilitates the extraction of many measures from the each set of data. Although exercised here only on plain-weave laminates, the general approach probably is applicable to composite materials of various woven-reinforcement geometries (subject to the restriction that a significant portion of each yarn shape lie in one plane).

Sets of yarn-shape data from samples of a plain-weave carbon-carbon laminates illustrate the rich quantity and variety of information that can be generated. It seems clear, from the Background discussion, that such information would be useful to the implementation of existing mechanics models, and would motivate development of improved models. Differences in yarn shape among similar materials, and some of the anomalies found in yarn-shape distributions, suggest that sampling yarn-shape parameters may also be useful as a quality control tool.

More work is needed to develop compact ways of reporting yarn-shape and nesting data, in forms useful for property prediction, micromechanics modeling, and quality control. Modelers, on the other hand, must be willing to accept the statistical nature of microstructure, and build models that accommodate distributed values. More experimental correlations between measures of yarn

shape and composite properties are needed. Work is also needed to identify how details of yarn morphology are established during composite fabrication. The ability to efficiently quantify yarn shape is a necessary prelude to these suggested efforts.

Acknowledgement

This work was sponsored by the Office of Naval Research under contract N00014-82-C-0405; the work at Clarkson University was supported by a subcontract from Jortner Research and Engineering. The authors thank Dr. L. H. Peebles, Jr., ONR's scientific officer, for his interest and encouragement.

References

[1] Hearle, J.W.S.; Grosberg, P.; Backer, S, eds.; *Structural Mechanics of Fibers, Yarns, and Fabrics, vol. 1*; Wiley-Interscience, NY 1969.

[2] Pierce, F.T.; *J. Textile Inst.*; 28, 1937.

[3] Olofsson, B.; "A General Model of a Fabric as a Geometric-Mechanical Structure"; *J. of the Textile Institute Trans.*; 55, pp. 541-557; 1964.

[4] Kawabata, S.; "Non-linear Mechanics of Woven and Knitted Materials", in *Textile Structural Composites*; Chou, TW.; Ko, F.K, ed.; Elsevier, NY,; pp 67-116; 1989.

[5] Stubbs, N.; "Elastic and Inelastic Responses of Coated Fabrics to Arbitrary Loading Paths" in *Textile Structural Composites*; Chou, TW.; Ko, F.K, ed.; Elsevier, NY,; pp 331-351; 1989.

[6] Chou, T-W; "Review of Flexible Composites"; *J. Materials Sci.*; 24; pp. 761-783; 1989.

[7] Bishop, S.M.; " Strength and Failure of Woven Carbon-fiber Reinforced Plastics for High Performance Applications" in *Textile Structural Composites*; Chou, TW.; Ko, F.K, ed.; Elsevier, NY,; pp 173-208; 1989.

[8] Jortner, J., "A Model for Predicting Thermal and Elastic Constants of Wrinkled Regions in Composite Materials" in *Effects of Defects in Composite Materials*; ASTM STP 836, pp.217-236, 1984.

[9] Chou, T-W, and Ishikawa, T.; "Analysis and Modeling of Two-Dimensional Fabric Composites" in *Textile Structural Composites*; Chou, TW.; Ko, F.K, ed.; Elsevier, NY,; pp 209-264; 1989.

[10] Zhang, Y. C., and Harding, J., "A Numerical Micromechanics Analysis of the Mechanical Properties of a Plain Weave Composite", Report OUEL 1760/89, University of Oxford, 1989.

[11] Whitcomb, John D., "Three-Dimensional Stress Analysis of Plain Weave Composites", Report NASA TM-101672, NASA Langley Research Center, November 1989.

[12] Jortner, J.; "A Model for Nonlinear Stress-Strain Behavior of 2D Composites with Brittle Matrices and Wavy Yarns" in *Advances in Composite Materials*; S.S. Wang and Y.D.S. Rajapakse, eds.; ASME AMD-Vol. 82; pp 131-146; 1986.

[13] Jortner, J., "Nonlinear and Bimodular Stress-Strain Behavior of Elastic Unidirectional Composites at Small Strain", *Proc. 4th Japan-US Conf. Composite Materials*; Technomic Publishing Co., pp.857-866, 1989.

[14] Jortner, J.; "Effects of Crimp Angle on the Tensile Strength of a Carbon-Carbon Laminate" in *Proceedings of the Symposium on High Temp. Composites*; Technomic Publishing Co; pp. 243-251, 1989.

[15] Pollock, P.;"Tensile Failure in 2-D Carbon-Carbon Composites"; *Carbon*; 28; pp. 717-732; 1990.

[16] Jortner, J., "Microstructure of Cloth-Reinforced Carbon-Carbon Laminates"in *Sixth Annual Conf. Materials Technology*, M. Genisio, Ed; Southern Illinois University at Carbondale, pp. 51-70, 1990.

[17] Dongarra, J.J., et.al., "LINPACK Users' Guide", Soc. of Industrial and Applied Mathematics (SIAM), 1979.

[18] DeHoff, R.T.; Rhines, E.T.; *Quantitative Microscopy*; McGraw Hill, NY; 1968.